

Relative dispersion of particle pairs in turbulent channel flow[☆]

J.I. Polanco^{a,*}, I. Vinkovic^a, N. Stelzenmuller^b, N. Mordant^b, M. Bourgoin^c

^aLaboratoire de Mécanique des Fluides et d'Acoustique, UMR 5509, Ecole Centrale de Lyon, CNRS, Université Claude Bernard Lyon 1, INSA Lyon, 36 av. Guy de Collongue, F-69134 Ecully, France

^bLaboratoire des Écoulements Géophysiques et Industriels, Université Grenoble Alpes & CNRS, Domaine Universitaire, CS 40700, F-38058 Grenoble, France

^cLaboratoire de Physique, École Normale Supérieure de Lyon, Université de Lyon, CNRS, 46 Allée d'Italie, F-69364 Lyon, France

Abstract

Lagrangian tracking of particle pairs is of fundamental interest in a large number of environmental applications dealing with contaminant dispersion and passive scalar mixing. The aim of the present study is to extend the observations available in the literature on relative dispersion of fluid particle pairs to wall-bounded turbulent flows, by means of particle pair tracking in direct numerical simulations (DNS) of a turbulent channel flow. The mean-square change of separation between particle pairs follows a clear ballistic regime at short times for all wall distances. The Eulerian structure functions governing this short-time separation are characterised in the channel, and allow to define a characteristic time scale for the ballistic regime, as well as a suitable normalisation of the mean-square separation leading to an overall collapse for different wall distances. Through fluid particle pair tracking backwards and forwards in time, the temporal asymmetry of relative dispersion is illustrated. At short times, this asymmetry is linked to the irreversibility of turbulence, as in previous studies on homogeneous isotropic flows. The influence of the initial separation (distance and orientation) as well as the influence of mean shear are addressed. By decomposing the mean-square separation into the dispersion by the fluctuating velocity field and by the average velocity, it is shown that the influence of mean shear becomes important at early stages of dispersion close to the wall but also near the channel centre. The relative dispersion tensor Δ_{ij} is also presented and particularly the sign and time evolution of the cross-term Δ_{xy} are discussed. Finally, a ballistic cascade model previously proposed for homogeneous isotropic turbulence is adapted here to turbulent channel flows. Preliminary results are given and compared to the DNS. Future developments and assumptions in two particle stochastic models can be gauged against the issues and results discussed in the present study.


Keywords: pair dispersion, inhomogeneous turbulence, channel flow, Lagrangian turbulence, direct numerical simulation

1. Introduction

The transport and mixing of passive components by turbulent flows are commonly encountered in a large number of environmental and industrial applications. Many atmospheric pollution studies have investigated contaminant dispersion in the context of Lagrangian tracking of single particles (Hoffmann et al., 2016; Fung et al., 2005; Angevine et al., 2013). In these studies, mesoscale meteorological models are often coupled with a Lagrangian particle dispersion model providing a numerical method for simulating the dispersion of passive pollutants in the atmosphere by means of a large ensemble of Lagrangian particles moving with the modelled flow velocity field (Fung et al., 2005). Recently, relative displacement measurements from balloons and drifters have been conducted both in the atmosphere and the ocean (Lumpkin and Elipot, 2010; LaCasce, 2010; Koszalka et al., 2009).

Relative pair dispersion is of theoretical interest because particle pairs simultaneously sample the velocity field at different positions. In fluid flows, the short-term mean-square difference between tracer particle velocities is equivalent to the second-order Eulerian velocity structure function, which is related to the turbulent kinetic energy spectrum. The turbulent kinetic energy at a particular scale determines how a tracer cloud is stirred relative to its centre of mass.

In the last few decades, advances in experimental techniques and computational power have enabled the characterisation of particle trajectories and relative pair dispersion in canonical turbulent flows. Most of these studies have dealt with fluid tracers in homogeneous isotropic turbulence (HIT) and have led to a greatly increased understanding of the Lagrangian properties of turbulent flows (Toschi and Bodenschatz, 2009), and in particular, of the mechanisms of transport and diffusion of tracer particles in isotropic flows. A review on recent advances in experiments, direct numerical simulations (DNS) and theoretical studies on particle pair dispersion has been provided by Salazar and Collins (2009), additionally to the review of Sawford (2001) on two-particle Lagrangian stochastic models. As described by Sawford (2001), particle pair Lagrangian stochastic models are

[☆]  This work is licensed under a Creative Commons CC BY-NC-ND 4.0 license (<https://creativecommons.org/licenses/by-nc-nd/4.0/>)

*Corresponding author

Email addresses: juan-ignacio.polanco@univ-lyon1.fr (J.I. Polanco), ivana.vinkovic@univ-lyon1.fr (I. Vinkovic)

a suitable tool for predicting dispersion of contaminant plumes in turbulence, since separation statistics of particle pairs can be directly related to the concentration covariance and to the dissipation of scalar fluctuations.

Fewer studies have dealt with particle pair dispersion in anisotropic and inhomogeneous turbulence, which is however ubiquitous in atmospheric flows. In particular, most real flows are characterised by the presence of mean shear or solid boundaries, which effectively suppress the movement of the fluid in the wall normal direction. This results in turbulent flows that are anisotropic due to the presence of a mean shear, and inhomogeneous because of confinement by the walls. Near the walls, turbulent fluctuations are mainly described by the formation of large-scale organised structures that are elongated in the mean flow direction (Smits et al., 2011; Stanislas, 2017).

As first described by Richardson (1926), turbulence can greatly enhance the pair separation process. In his seminal paper, Richardson proposed that the separation of two tracers in a turbulent flow can be described (in a statistical sense) by a diffusive process, with a non-constant diffusion coefficient $K(D)$ which depends on the separation D between the two particles. When D is within the inertial subrange of a turbulent flow (that is, much larger than the dissipative scale η and much smaller than the scale of the largest turbulent eddies L), Richardson found from measurements that the diffusion coefficient $K(D)$ is proportional to $D^{4/3}$, which is since known as Richardson's 4/3 law. As later shown by Obukhov (1941), the same relation can be derived from dimensional arguments in the framework of K41 local isotropy theory (Kolmogorov, 1941). This requires the additional hypothesis that there is a loss of memory of the initial condition, such that the initial pair separation D_0 no longer plays a role in the separation process (Batchelor, 1950). As a consequence, the mean-square separation between two particles is expected to grow as $\langle D^2(t) \rangle = g\varepsilon t^3$ when D is in the inertial subrange, where ε is the mean turbulent energy dissipation rate, and the non-dimensional coefficient g , known as Richardson's constant, is expected to have an universal value.

As mentioned above, the initial separation D_0 must be taken into account at short separation times (Batchelor, 1950). This dependency can be expressed as a short-term ballistic growth of the mean-square separation:

$$\langle \mathbf{R}(t)^2 \rangle = \langle (\mathbf{D}(t) - \mathbf{D}_0)^2 \rangle = \langle \delta \mathbf{v}_0^2 \rangle t^2 \quad \text{for } t \ll t_B, \quad (1)$$

where $\mathbf{D}(t)$ is the instantaneous particle separation vector and $\mathbf{D}_0 = \mathbf{D}(0)$, $\delta \mathbf{v}_0$ is the initial relative velocity between the particles, and t_B is a characteristic time scale of the ballistic regime, that may be related to the characteristic time scales of the turbulent flow. Equation (1) can be obtained from the Taylor expansion of $\mathbf{D}(t)$ about $t = 0$. The average $\langle \cdot \rangle$ is taken over an ensemble of particle pairs initially separated by \mathbf{D}_0 . In HIT, if $D_0 = |\mathbf{D}_0|$ is within the inertial subrange, the ballistic time t_B may be taken as proportional to the eddy-turnover time at the scale D_0 (also referred to as the Batchelor time scale), i.e. $t_E = D_0^{2/3} \varepsilon^{-1/3}$ (Batchelor, 1950).

By following two million passive tracers in a direct numerical simulation, Biferale et al. (2005) found high levels of intermittency for travel times up to ten Kolmogorov time scales in pair

dispersion statistics in HIT at $Re_\lambda = 260$. The authors proposed an alternative method for calculating Richardson's constant by computing statistics at fixed separations. Also in HIT, Rast and Pinton (2011) studied pair dispersion by analysing the time scale t_B during which particle pairs remain together before the separation increases significantly in a simplified point-vortex flow model. The authors suggested that pair separation may be understood as an average over separations which follow Richardson's scaling but each over a fluctuating time delay t_B .

Relative dispersion in HIT is known to be a time-asymmetric process. That is, when fluid particles are tracked backwards in time (starting from an imposed *final* separation), they tend to separate faster than in the forward case (Sawford et al., 2005; Berg et al., 2006; Buaria et al., 2015). Recently, Jucha et al. (2014) and Bragg et al. (2016) linked this temporal asymmetry at short times to the irreversibility of turbulence, which can be understood as the directionality of the turbulent energy cascade (from large to small scales in 3D turbulence). Moreover, Bragg et al. (2016) compared backward and forward in time dispersion statistics for inertial particle pairs. They found that the ratio of backwards to forwards in time mean-square separation may be up to an order of magnitude larger for inertial particles than for fluid particles in isotropic turbulence. Inertial particles were found to experience an additional source of irreversibility arising from the non-local contribution of their velocity dynamics.

Richardson's super-diffusive regime described above requires the existence of an intermediate time range in which the following two conditions are simultaneously satisfied: (1) the initial separation has been forgotten ($t \gg t_B$), and (2) particle separation remains small enough such that their trajectories are still correlated ($D(t) \ll L$). The second condition is equivalent to $t \ll T_L$, where T_L is the Lagrangian integral time scale (Salazar and Collins, 2009). This implies large scale separation which occurs for turbulent flows at very high Reynolds numbers.

In inhomogeneous and anisotropic turbulent flows, the relative dispersion problem is more complex, since the statistics depend not only on the magnitude, but also on the direction of the initial particle separation vector \mathbf{D}_0 and on the initial particle position. Moreover, particles do not separate equally in each direction. Therefore, the mean-square separation $\langle \mathbf{R}(t)^2 \rangle$ can be generalised into a dispersion tensor $\Delta_{ij}(t) = \langle R_i(t)R_j(t) \rangle$ (Batchelor, 1952) containing more than a single independent component (as opposed to the isotropic case).

The case of a homogeneous shear flow was studied by direct numerical simulations (DNS) by Shen and Yeung (1997). The authors observed that particles separate faster when they are initially oriented in the cross-stream direction, that is, when they are in regions of different streamwise mean velocities. Moreover, regardless of their initial separation vector, over time their mean-square separation becomes larger in the streamwise direction than in the spanwise and cross-stream directions. Celani et al. (2005) studied the competition between the effects of turbulence fluctuations and a linear mean shear on particle separation using a simple analytical model. They proposed the existence of a temporal transition between a first stage of separation, where turbulent fluctuations dominate and Richardson's law can be expected to hold, and a second stage where mean shear becomes

dominant. The transition is expected to happen at a crossover time which is proportional to the characteristic time scale of the mean shear.

More recently, Pitton et al. (2012) studied the separation of inertial particle pairs in a turbulent channel flow using DNS at a friction Reynolds number $Re_\tau = 150$. Results for inertial particles were compared to fluid tracers. The authors observed that mean shear induces a super-diffusive regime at large times, when particle separation becomes of the order of the largest scales of the flow. Arguably due to an insufficient separation of scales, Richardson’s regime was not clearly identified. Pitton et al. (2012) removed the effect of mean shear by tracking particles which follow the fluctuating velocity field. They found that, although pair separation is importantly reduced at long times compared to the case with mean shear, separation in the streamwise direction remains dominant over the wall-normal and spanwise separations.

The DNS of Pitton et al. (2012) revealed the fundamental role played by inertial particle-turbulence interactions at small scales in the initial stages of pair separation. The authors found a super-diffusive pair dispersion of inertial particles in channel flow. This super-diffusion at short times exhibited strong dependency on particle inertia, and persisted even when the influence of mean shear was removed by the procedure described in the previous paragraph. Using DNS and Lagrangian tracking of inertial particles, Sardina et al. (2012) studied turbulence-induced wall accumulation of inertial particles (turbophoresis) and small-scale clustering. The authors showed that for inertial particles, the clustering intensity in the near-wall region is directly correlated with the strength of the turbophoretic drift. In the case of inertial particles, clustering and near-wall accumulation are expected to strongly influence particle pair dispersion statistics. Lashgari et al. (2016) used a DNS coupled with immersed boundary methods to study the collision kernel and relative pair statistics of finite-size solid particles in turbulent channel flows for a wide range of volume fractions and Reynolds numbers. The authors found that the particle relative velocity and clustering are clearly influenced by inertia and particle concentration. Recently, Fornari et al. (2018) studied polydispersed particle pair statistics also by DNS and an immersed boundary method accounting for finite-size effects. The radial distribution function and the average normal relative velocity between two approaching particles were computed in order to estimate the collision kernel. Collision statistics were found to be dominated by the behaviour of smaller particles. Fornari et al. (2018) calculated that on average inertial particles stay during $t = 2.5h/U_0$ within a radial distance of one particle radius, indicating that for polydispersed inertial particles long times are needed before a particle pair breaks.

The aim of this study is to extend the available literature on relative dispersion of fluid particle pairs in anisotropic and inhomogeneous turbulent flows. Pair dispersion statistics are obtained here by DNS in a turbulent channel flow at a Reynolds number based on the friction velocity, $Re_\tau \approx 1440$. Particle pairs are tracked backwards and forwards in time to characterise the time asymmetry of relative dispersion. New results show that a simple ballistic dynamics accurately reproduces the initial pair separation regime and the short-term temporal asymmetry of

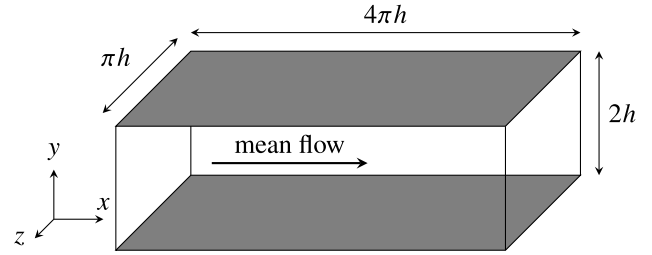


Figure 1: Channel dimensions and coordinate system.

relative dispersion, regardless of the local turbulence properties (anisotropy, turbulent structures) in the channel. Based on this description, time scales relevant to relative dispersion are discussed and a suitable normalisation is proposed, leading to similarity of mean-square separation statistics for initial wall distances $y_0^+ \gtrsim 60$. The influence of mean shear and of the initial distance and orientation of the particle pair separation are addressed in this work. Finally, a simple ballistic cascade model accounting for the influence of mean shear is presented. The model reproduces the main features of the initial stages of dispersion as observed by DNS. Suitable data and results are provided with which the assumptions and predictions of two-particle stochastic models (Sawford, 2001) can be tested. Particularly, the direct numerical simulation results discussed here may give more detailed information against which future developments and modelling assumptions can be gauged.

The structure of the paper is the following. We first present the numerical approach (Section 2). In Section 3 the mean-square separation evolution in time is discussed. A characteristic time scale of the ballistic regime and a normalisation of the relative dispersion at different wall distances are proposed. The influence of mean shear is addressed in Section 4. The analysis of the relative dispersion tensor is given in Section 5. Finally, an adaptation of the ballistic cascade model initially proposed by Bourgoin (2015) to the case of a turbulent channel flow is presented in Section 6 together with preliminary results and comparisons with DNS. Section 7 is devoted to the conclusion.

2. Numerical approach

We perform direct numerical simulations to study the relative dispersion of fluid particles in a turbulent channel flow between two parallel walls separated by a distance $2h$, as illustrated in Fig. 1. The Reynolds number based on the mean velocity U_0 at the channel centre is $Re = U_0 h / \nu = 34\,000$, where ν is the kinematic viscosity of the fluid. This corresponds to a friction Reynolds number $Re_\tau = u_\tau h / \nu \approx 1440$, where $u_\tau = (\tau_w / \rho)^{1/2}$ is the friction velocity associated to the mean shear at the walls τ_w . In the following, the superscript + is used to indicate physical quantities normalised by u_τ and ν .

In the DNS, the Navier-Stokes equations are solved using a pseudo-spectral method (Buffat et al., 2011). The solver is coupled with Lagrangian tracking of fluid particles. The numerical domain is periodic in the streamwise (x) and the spanwise (z) directions, where the solution is decomposed into Fourier

modes. In the wall-normal (y) direction, a Chebyshev expansion is applied and no-slip boundary conditions are enforced at the channel walls. As in Stelzenmuller et al. (2017), the domain size is $L_x \times L_y \times L_z = 4\pi h \times 2h \times \pi h$, and the velocity field is decomposed into $2048 \times 433 \times 1024$ modes. In physical space, this corresponds to a grid spacing $\Delta x^+ = 8.9$ and $\Delta z^+ = 4.4$ in the periodic directions, while the wall-normal spacing Δy^+ ranges from 0.04 at the wall to 10.5 at the channel centre. The Eulerian velocity field $\mathbf{u}(\mathbf{x}, t)$ is advanced in time using an explicit second-order Adams-Bashforth scheme with a time step $\Delta t^+ = 0.033$. The acceleration field is obtained in the Eulerian frame from the resolved velocity according to $\mathbf{a} = \frac{\partial \mathbf{u}}{\partial t} + \nabla(\mathbf{u}^2/2) + (\nabla \times \mathbf{u}) \times \mathbf{u}$. Fluid particle tracking is achieved by interpolation of the velocity and acceleration fields at each particle position using third-order Hermite polynomials. Particles are advanced in space at each iteration using the same Adams-Bashforth scheme as for the Eulerian field. Particle positions, velocities and accelerations are stored every 10 iterations (every $\Delta t_p^+ = 0.33$). The total simulation time is $T_{\text{sim}}^+ \approx 1.7 \times 10^4$, or equivalently $T_{\text{sim}} U_0/h \approx 279$ based on the mean centreline velocity U_0 .

Dispersion statistics are obtained from two different sets of fluid particles, labelled DS1 and DS2. The dataset DS1 consists of 2×10^6 particles initialised at random positions in the domain. During post-processing, particle pairs are identified at chosen times t_0 according to the criterion described further below, and relevant statistics are computed over the temporal range $t \in [t_0 - T/2, t_0 + T/2]$. This naturally allows to obtain backwards and forwards dispersion statistics, and is similar to the approach described in Berg et al. (2006) and more recently in Buaria et al. (2015). The temporal window length is chosen as $T^+ \approx 1.1 \times 10^4$, and the spacing between two reference times t_0 is taken as $\Delta t_0^+ \approx 1.3 \times 10^3$.

The criterion for particle pair identification in dataset DS1 is as follows. Pairs separated by $|\mathbf{D}_0| < D_0^{\text{max}}$ at t_0 are identified, such that their centroids are located within bins of wall-normal distance $y = y_0 \pm \delta y/2$. The maximum pair separation is taken as $D_0^{\text{max}} = 16\eta$, where the Kolmogorov length scale η , which varies with wall distance, is defined as $\eta = (v^3/\varepsilon)^{1/4}$. Here, the mean turbulent energy dissipation rate is estimated as $\varepsilon = \overline{v(\partial_j u_i')(\partial_j u_i')}$, where $\mathbf{u}'(\mathbf{x}, t)$ is the instantaneous fluctuating velocity field. The mean dissipation profile $\varepsilon(y)$ has been computed in the Eulerian frame from the same DNS. Pair dispersion statistics are computed over sets of particle pairs initialised at the same reference wall distance y_0 . In wall units, the positions $y_0^+ = 20, 60, 200, 600$ and 1000 are chosen (the channel centre is at $y^+ = 1440$). The bin widths are taken as $\delta y = 8\eta$. The Kolmogorov length scale ranges from $\eta^+ \approx 1.72$ at $y_0^+ = 20$ to $\eta^+ \approx 5.31$ at $y_0^+ = 1000$. Consequently, particles in the $y_0^+ = 20$ group may initially be located within $0 \leq y^+ \leq 40$. Due to the evolution of η with wall distance, the total number of identified particle pairs varies from roughly 1.7×10^4 samples at $y_0^+ = 20$, to 1.5×10^6 samples at $y_0^+ = 1000$. The dataset DS1 has already been used to study the acceleration of Lagrangian tracers in a turbulent channel flow at the same Reynolds number (Stelzenmuller et al., 2017).

Particles in dataset DS2 are initialised at chosen locations in

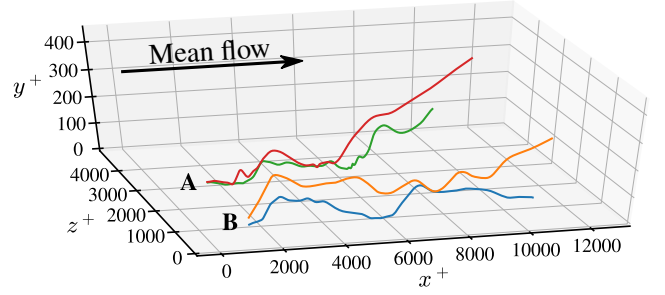


Figure 2: Sample trajectories of two pairs of particles from dataset DS2. Trajectories are shown over $t^+ = 600$. In both cases, the initial wall distance is $y_0^+ = 18$ and the initial separation is $D_0 = 16\eta$ ($D_0^+ = 27$). The pairs **A** and **B** are initially oriented in the spanwise (z) and wall-normal (y) directions, respectively.

order to characterise the influence of the initial configuration of the pairs on relative dispersion. Each initial configuration is defined by 3 parameters: the initial wall distance y_0 of one of the particles in the pair; the separation magnitude D_0 between the two particles; and the orientation of the pair separation \mathbf{e}_0 , so that their initial separation vector is $\mathbf{D}_0 = D_0 \mathbf{e}_0$. In the simulations, we chose 10 initial wall distances y_0^+ ranging from 3 to 1440, combined with separations $D_0/\eta = 1, 4, 16$ and 64 , and orientations in the three Cartesian directions ($\mathbf{e}_0 \in \{\mathbf{e}_x, \mathbf{e}_y, \mathbf{e}_z\}$). This results in 120 different initial configurations. For each parameter combination, the size of the statistical sample (i.e. the number of particle pairs) is roughly 20 000. Only forward dispersion statistics are obtained from this dataset. Applying the same approach to backward dispersion would require the storage of an exceedingly large amount of Eulerian velocity fields, with a prohibitive cost in terms of storage memory (Sawford et al., 2005).

In Fig. 2, the trajectories of two pairs of particles initialised near the wall are shown. At the initial time, both particle pairs differ only on the orientation of their initial separation, with pair A being oriented in the spanwise direction, and pair B in the wall-normal direction. At the initial stage of separation, mean shear has no influence on the separation of pair A, since both particles are at the same wall distance y^+ . For relatively small wall-normal particle separations D_y , the influence of turbulent fluctuations on separation statistics dominates over mean shear. The case of pair B is different, since the two particles are initially in regions of different mean velocity, and therefore shear effects are important from the start. As can be seen from Fig. 2, under the influence of mean shear, particles in pair B separate faster than in pair A following their release, reaching larger separations D at short times. At larger times, the influence of the initial orientation is less noticeable, as observed from comparable separations of pairs A and B at the end of all trajectories ($t^+ = 600$).

3. Mean-square separation

Particle pair separation statistics are considered here in a fully-developed wall-bounded turbulence by analysing the mean-square change of separation between two particles, $\langle \mathbf{R}(t)^2 \rangle = \langle (\mathbf{D}(t) - \mathbf{D}_0)^2 \rangle$, where $\mathbf{D}(t)$ is the instantaneous separation vector,

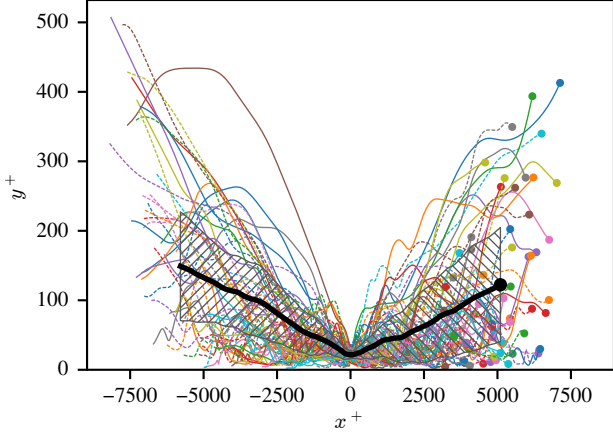


Figure 3: Illustration of the Lagrangian averaging procedure. Thin curves represent trajectories of sample particle pairs with centroids located at $y_0^+ = y_0^+ \pm \delta y^+ / 2$ for a reference time $t = 0$ (here $y_0^+ = 20$ and $\delta y^+ = 14$). The initial pair separation is $D_0 < 16\eta$ ($D_0^+ \lesssim 27$). Trajectories are shifted in the streamwise direction so that the particle pair centroids are at $x(t = 0) = 0$. The thick curve represents the Lagrangian average of the particle positions $\langle \mathbf{x}(t) \rangle$. The hatched area represents the standard deviation of the wall-normal particle pair separation $D_y(t)$, and is defined as the area between the curves $\langle y(t) \rangle \pm 0.5 \langle D_y^2(t) \rangle^{1/2}$. Trajectories are shown for time lags $t^+ \in [-400, 400]$.

and $\mathbf{D}_0 = \mathbf{D}(0)$ is the initial separation. In HIT, statistics of \mathbf{R} only depend on two parameters: the initial particle separation distance $D_0 = |\mathbf{D}_0|$ and time t . In channel flow, as a consequence of anisotropy and inhomogeneity, such statistics also depend on the initial orientation of the pair \mathbf{e}_0 (such that $\mathbf{D}_0 = D_0 \mathbf{e}_0$) and on the initial wall-normal position y_0 of one of the particles in the pair (such that the wall-normal position of the other particle is $y_0 + \mathbf{D}_0 \cdot \mathbf{e}_y$). Here, $\langle \cdot \rangle$ denotes an average over pairs of particles initially located at the same y_0 and with the same initial orientation and separation \mathbf{D}_0 . In Fig. 3, this Lagrangian averaging procedure is illustrated for sample particle pairs initially located at $y_0^+ \approx 20$, and with initial separations $D_0 < 16\eta$. The represented Lagrangian statistics are the mean particle position $\langle \mathbf{x}(t) \rangle$ and the wall-normal mean-square separation $\langle D_y^2(t) \rangle$.

Figure 4 shows the time evolution of the mean-square change of separation $\langle \mathbf{R}^2 \rangle$ for initial separations $D_0 < 16\eta$, and for different initial positions y_0 (dataset DS1). In this case, statistics are averaged among all initial separation vectors \mathbf{D}_0 within a sphere of radius 16η . At short times, the ballistic regime predicted by Eq. (1) is found for both backward and forward dispersion, and for all wall distances. Following this initial regime, a growing gap is observed at intermediate times between backward and forward dispersion, with the former being faster than the latter. This is qualitatively consistent with observations in 3D HIT, described in the introduction (Sawford et al., 2005; Berg et al., 2006; Jucha et al., 2014; Bragg et al., 2016).

In the following subsections, first the short-time ballistic dispersion regime is analysed. By considering the Taylor expansion of the separation at short times, the influence of the second-order Eulerian velocity structure function and the crossed velocity-acceleration structure function is emphasised. The evolution of these structure functions is described in Section 3.2. Then, in

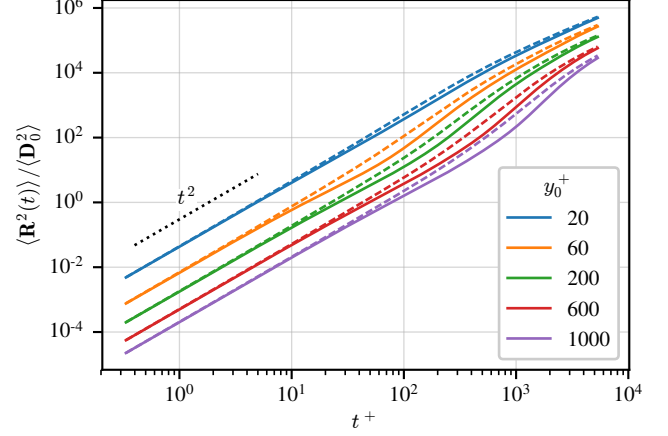


Figure 4: Backward and forward mean-square change of separation $\langle \mathbf{R}^2 \rangle$ normalised by the initial mean-square separation $\langle D_0^2 \rangle$. Particle pairs are initially separated by $D_0 < 16\eta$ (dataset DS1). Different colours correspond to different initial wall distances y_0^+ . Solid lines: forward dispersion. Dashed lines: backward dispersion.

Section 3.3, a suitable definition of the ballistic time scale is presented, enabling the introduction of the normalised mean-square separation in Section 3.4. The temporal asymmetry of pair dispersion statistics is then addressed in the case of turbulent channel flow (Section 3.5), as well as the influence of the initial separation distance and orientation (Section 3.6).

3.1. Short-time dispersion

To understand the observed short-time ballistic regime and the deviation that follows, we consider the Taylor expansion of the separation between two particles at short times, $\mathbf{D}(t) = \mathbf{D}_0 + \delta \mathbf{v}_0 t + \frac{1}{2} \delta \mathbf{a}_0 t^2 + O(t^3)$. Here $\delta \mathbf{v}_0$ and $\delta \mathbf{a}_0$ are the relative particle velocity and acceleration, respectively, at $t = 0$. As a result, the short-time mean-square separation is expressed as

$$\langle \mathbf{R}^2 \rangle(y_0, \mathbf{D}_0, t) = \langle \delta \mathbf{v}_0^2 \rangle t^2 + \langle \delta \mathbf{v}_0 \cdot \delta \mathbf{a}_0 \rangle t^3 + O(t^4) \quad \text{for } t \ll t_B, \quad (2)$$

where the characteristic time scale t_B describes the duration of the short-time regime. At the leading order, the mean-square separation follows the ballistic regime (Batchelor, 1950), during which particles travel at their initial velocities. The mean-square initial relative velocity $\langle \delta \mathbf{v}_0^2 \rangle$ is equivalent to the second-order Eulerian structure function $S_2(\mathbf{x}_0, \mathbf{D}_0) = \overline{\delta \mathbf{u}^2(\mathbf{x}_0, \mathbf{D}_0)} = \overline{[\mathbf{u}(\mathbf{x}_0 + \mathbf{D}_0, t) - \mathbf{u}(\mathbf{x}_0, t)]^2}$, where $\mathbf{u}(\mathbf{x}, t)$ is the Eulerian velocity, and \mathbf{x}_0 is the position of the first particle in the pair. In channel flows, due to statistical homogeneity in the streamwise and spanwise directions, the dependency of S_2 on \mathbf{x}_0 reduces to a dependency on the wall-normal distance y_0 . In HIT, S_2 only depends on the separation $D_0 = |\mathbf{D}_0|$. Moreover, when this separation is within the inertial subrange, K41 theory predicts the well-known relation $S_2(D_0) = \frac{11}{3} C_2 (\varepsilon D_0)^{2/3}$, where C_2 is Kolmogorov's constant for the longitudinal second-order velocity structure function, with $C_2 \approx 2.1$ (Sreenivasan, 1995; Pope, 2000).

At the next order, the ballistic term in Eq. (2) is corrected by a t^3 term whose coefficient $\langle \delta \mathbf{v}_0 \cdot \delta \mathbf{a}_0 \rangle$ is equal to the crossed velocity-

acceleration structure function $S_{au}(\mathbf{x}_0, \mathbf{D}_0) = \overline{\delta \mathbf{u} \cdot \delta \mathbf{a}(\mathbf{x}_0, \mathbf{D}_0)}$. Under the conditions of local homogeneity and stationarity, if the spatial increment D_0 is within the inertial subrange, the velocity-acceleration structure function is given by

$$S_{au}(\mathbf{x}_0, \mathbf{D}_0) = -(\varepsilon(\mathbf{x}_0) + \varepsilon(\mathbf{x}_0 + \mathbf{D}_0)) = -2\bar{\varepsilon}(\mathbf{x}_0, \mathbf{D}_0), \quad (3)$$

where $\bar{\varepsilon}$ is the turbulent dissipation rate averaged among the two probed positions (Mann et al., 1999; Hill, 2006). This relation is exact in the limit of infinite Reynolds numbers, and is the Lagrangian equivalent of Kolmogorov's 4/5 law (Frisch, 1995). The negative sign of S_{au} is associated with the direction of the turbulent cascade, from large to small scales in 3D turbulence. Thus, under the assumptions for Eq. (3), the t^3 term of Eq. (2) is negative for forward dispersion ($t > 0$) and positive for backward dispersion ($t < 0$). This explains the short-time temporal asymmetry of relative dispersion in isotropic flows (Jucha et al., 2014).

3.2. Structure functions S_2 and S_{au}

The evolution of the structure functions introduced above with wall distance and with spatial increment is investigated in order to describe the short-time dispersion regime given by Eq. (2). To our knowledge, few studies in literature have dealt with Eulerian structure functions in wall-bounded turbulent flows. Moreover, studies characterising the crossed velocity-acceleration structure function S_{au} in such flows are still lacking. Existent works have focused on the logarithmic region of boundary layers, and have mainly studied the second-order streamwise velocity structure function $S_{xx}(y, \mathbf{D}) = \delta u_x^2(y, \mathbf{D})$ for streamwise separations, $\mathbf{D} = D\mathbf{e}_x$ (see e.g. Davidson and Krogstad, 2014; de Silva et al., 2015). Recently, Yang et al. (2017) proposed scalings for the complete fluctuating velocity structure function tensor $S'_{ij}(y, \mathbf{D}) = \delta u'_i \delta u'_j(y, \mathbf{D})$ in the logarithmic region, based on the attached-eddy model (Townsend, 1976). However, when considering spanwise separations ($\mathbf{D} = D\mathbf{e}_z$), their predicted scalings do not match the results obtained from channel flow DNS at moderate Reynolds number (Lozano-Durán and Jiménez, 2014).

We estimate S_2 and S_{au} across the channel from Lagrangian data at $t = 0$ when particles of dataset DS2 are released. The estimation is performed over all initial particle configurations, namely for a range of wall distances y_0 and spatial displacement vectors \mathbf{D}_0 . The evolution with wall distance of the velocity and velocity-acceleration structure functions, for different initial orientations and magnitudes of the separation vector, is given in Fig. 5. Since S_{au} is mostly negative (as expected in homogeneous flows), we plot $-S_{au}$.

In the near-wall region the structure functions display a strong dependency on the orientation of the displacement \mathbf{D}_0 . This anisotropy is due to wall confinement and the influence of mean shear. The latter only plays a role when the initial separation is in the wall-normal direction. For this orientation, S_2 is expected to be larger since it includes a contribution of the mean velocity increment $\delta U = U(y + D_y) - U(y)$, where $U(y)$ is the mean streamwise velocity across the channel. This is confirmed by the curves of Fig. 5. Moreover, near the wall S_2 is larger for

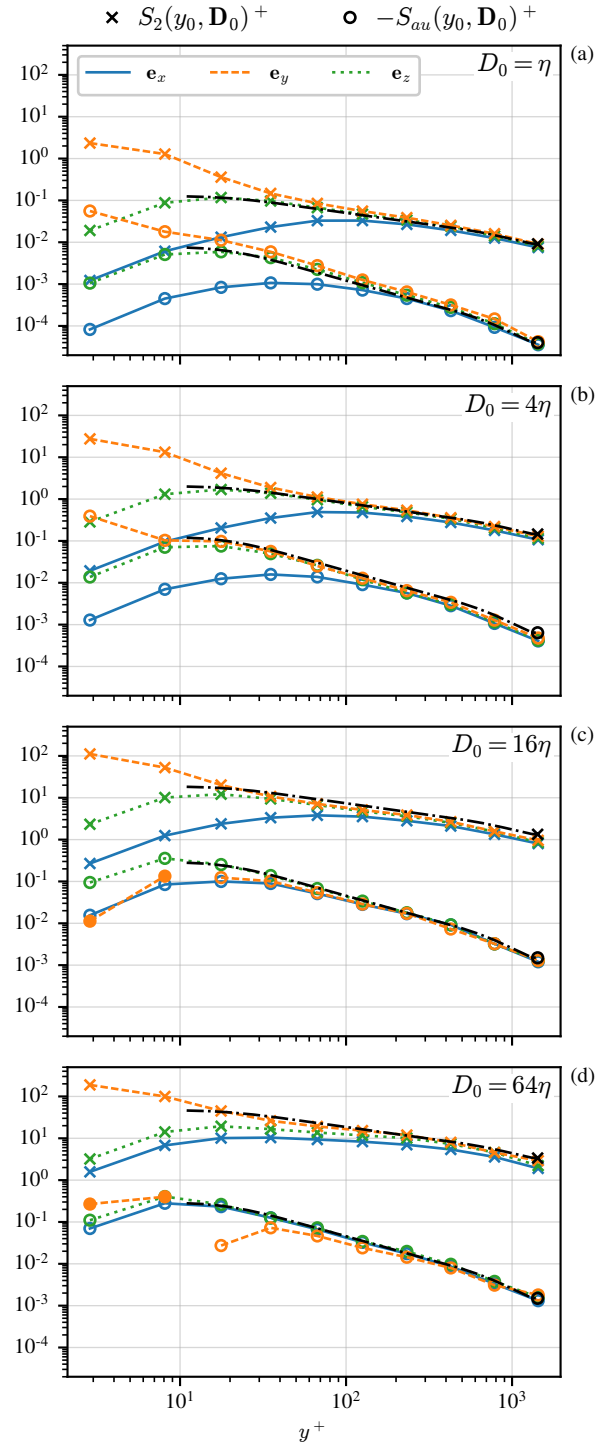


Figure 5: Structure functions $S_2(y_0, \mathbf{D}_0)$ (crosses) and $-S_{au}(y_0, \mathbf{D}_0)$ (circles) in wall units, for all initial configurations of dataset DS2. From top to bottom, $D_0/\eta = 1, 4, 16$ and 64 . Initial orientations are $\mathbf{e}_0 = \mathbf{e}_x$ (solid lines), \mathbf{e}_y (dashed lines) and \mathbf{e}_z (dotted lines). Filled circles represent positive values of S_{au} . Black dash-dotted lines represent isotropic estimations of S_2 and S_{au} . For small separations (subfigures a-b), a dissipation-range estimation is used, $S'_2 = \varepsilon D_0^2/(3\nu)$ and $S_{au} = \beta \varepsilon D_0^2/(3\eta^2)$, with $\beta = -0.16$. For large separations (subfigures c-d), an inertial-range estimation is used, $S_2 = \frac{11}{3} C_2 (\varepsilon D_0)^{2/3}$ and $S_{au} = -2\varepsilon$, with $C_2 = 2.1$.

spanwise than for streamwise displacements, with a difference that is more pronounced for smaller separations D_0 . This is due to the presence of streaks and quasi-streamwise vortices, which induce a fluctuating velocity field that is correlated for larger distances in the streamwise direction (see e.g. Robinson, 1991). Hence, the velocity increment between two points in the near-wall region is weaker if the points are aligned in the streamwise direction (since both points are likely to be found within the same coherent structure), than in the spanwise direction.

As shown in Fig. 5, the velocity-acceleration structure function S_{au} is also anisotropic near the wall. For small separations ($D_0/\eta = 1$ and 4), its behaviour is similar to that of S_2 , since its absolute value is larger for wall-normal displacements and smaller for streamwise displacements. As mentioned above, S_{au} is mostly negative. Positive values are obtained in a few extreme cases when one of the probed locations is at $y^+ < 10$ while the other is at $y^+ + D_{0y}^+$, with $D_{0y} \geq 16\eta$ ($D_{0y}^+ \gtrsim 25$). In these cases the velocity and acceleration increments describe the relation between the flow in the viscous sublayer (or the beginning of the buffer layer), and the beginning of the logarithmic region. Since these regions have very different dynamics, homogeneity is not expected to hold on the resulting two-point statistics. Furthermore, in these cases S_{au} is dominated by the scalar product between the mean velocity and mean acceleration increments, $\delta\mathbf{U} \cdot \delta\mathbf{A} = \delta U_x \delta A_x$. In the buffer layer and the beginning of the logarithmic region, the mean streamwise acceleration $A_x(y)$ is an increasing function of wall distance (Yeo et al., 2010; Stelzenmuller et al., 2017), similarly to the mean velocity $U_x(y) = U(y)$. This results in a positive product $\delta U_x \delta A_x$ when locations across the buffer layer are sampled.

Away from the wall, the structure functions become nearly independent of the displacement orientation, suggesting a return to isotropy towards the bulk of the channel. In general, this is observed for wall distances $y^+ \gtrsim 200$. Still, a slight difference persists for S_2 at nearly all wall distances, with the streamwise orientation resulting in a weaker structure function. This may be associated with the persistence of very-large-scale motions in the channel (VLSMs; Smits et al., 2011). A similar behaviour is observed for S_{au} at the smallest separations $D_0/\eta = 1$ and 4.

In Fig. 5, the S_2 profiles obtained from our DNS at small separations $D_0/\eta = 1$ and 4 are compared with the dissipation-range estimation for the fluctuating part of the structure function, $S_2' \sim \frac{1}{3} \overline{(\partial_j u_i')(\partial_j u_i')} D_0^2$, which is derived from the first-order Taylor expansion $\delta\mathbf{u}' \approx (\mathbf{D}_0 \cdot \nabla)\mathbf{u}'$ and the isotropy assumption. The estimation above can be expressed in terms of the mean turbulent dissipation rate $\varepsilon = \nu \overline{(\partial_j u_i')(\partial_j u_i')}$. For the two separations, the computed S_2 profiles closely match the prediction, suggesting that separations up to 4η are not within the inertial subrange. Similarly, the S_{au} profiles at separations η and 4η are compared to the dissipation-range estimation $S_{au} \sim \frac{1}{3} \overline{(\partial_j u_i)(\partial_j a_i)} D_0^2$. Dimensional considerations predict that $\overline{(\partial_j u_i)(\partial_j a_i)} = \beta \varepsilon / \eta^2$, with β a non-dimensional constant. The value $\beta = -0.16$ is found to fit the $\langle \delta\mathbf{v}_0 \cdot \delta\mathbf{a}_0 \rangle$ data at $D_0 = \eta$. For $D_0 = 4\eta$, the prediction slightly overestimates the results obtained from particle data in the bulk of the channel, hinting the beginning of the transition from dissipation to the inertial regime.

Furthermore, we compare the larger separations $D_0/\eta = 16$ and 64 with the inertial-range K41 prediction for locally isotropic turbulence $S_2(D_0) = \frac{11}{3} C_2 (\varepsilon D_0)^{2/3}$, where ε varies with wall distance. In the channel, the local isotropy condition may be expected to hold at large-enough wall distances. The obtained S_2 profiles accurately match the K41 prediction in the bulk of the channel. For spanwise separations, the estimation is accurate up to the near-wall region. Similarly, to verify the validity of relation (3), the obtained S_{au} profiles at separations 16η and 64η are compared with $-2\varepsilon(y)$. For non-zero wall-normal displacements D_y , one has $\varepsilon(y) \neq \tilde{\varepsilon}(y, D_y)$, so that the comparison is not exactly equivalent to Eq. (3) in the case of wall-normal displacements. Remarkably, the prediction holds almost exactly over a wide range of wall distances. This is especially true for spanwise displacements, for which a good agreement is found at nearly all wall distances.

3.3. Ballistic time scale

The most suitable definition of the initial ballistic regime duration t_B is discussed in this section. Originally, Batchelor (1950) assumed this time as proportional to the eddy-turnover time at scale D_0 , i.e. $t_E = D_0^{2/3} \varepsilon^{-1/3}$ (Frisch, 1995), when D_0 is in the inertial range. An alternative is to consider the time at which the t^2 and t^3 terms in Eq. (2) have the same magnitude, $t_0 = \langle \delta\mathbf{v}_0^2 \rangle / |\langle \delta\mathbf{v}_0 \cdot \delta\mathbf{a}_0 \rangle| = S_2(\mathbf{x}_0, \mathbf{D}_0) / |S_{au}(\mathbf{x}_0, \mathbf{D}_0)|$. This characteristic time may be approximated by the dissipation- or inertial-range predictions for the structure functions S_2 and S_{au} introduced in Section 3.2. For separations D_0 in the dissipation range, this approximation is given by $t_0^* = t_D = \tau_\eta / \beta$, where $\tau_\eta = (\nu / \tilde{\varepsilon})^{1/2}$ is the Kolmogorov time scale. For inertial-scale separations, the corresponding estimation is $t_0^* = t_I = \frac{11}{6} C_2 D_0^{2/3} \tilde{\varepsilon}^{-1/3}$, which is proportional to Batchelor's time scale.

The time scales t_0 and t_0^* are computed for each of the initial configurations of dataset DS2. In Fig. 6, the results are shown for all sets of particle pairs that were initially oriented in the spanwise direction. For separations $D_0/\eta = 1$ and 4, the dissipation-range form of t_0^* is plotted, while for $D_0/\eta = 16$ and 64, the inertial-range approximation is shown. Also shown are the mean shear time scale across the channel, $T_S(y) = (dU(y)/dy)^{-1}$ and the Lagrangian integral time scale $T_L(y)$, as obtained in Stelzenmuller et al. (2017). Because of anisotropy, a different Lagrangian integral time scale can be defined for each velocity component, $T_{L,i}$ for $i = 1, 2, 3$ (Stelzenmuller et al., 2017). Here, we take T_L as the quadratic mean among the three velocity components, $T_L^2 = \sum_i T_{L,i}^2 / 3$.

As shown in Fig. 6, the dissipation-range estimation $t_0^* = \tau_\eta / \beta$ matches the ballistic time t_0 over all wall distances for the smallest separation $D_0 = \eta$. For $D_0 = 4\eta$, there is still good agreement between both time scales, even though a weak departure from dissipation-range scaling is observed. This departure is consistent with observations in Section 3.2 regarding the validity of the dissipation-range estimation of S_{au} at $D_0 = 4\eta$. The agreement between t_0 and t_0^* shows the relevance of the characteristic dissipation time τ_η on the ballistic separation regime for small initial separations. For separations $D_0/\eta = 16$ and 64, t_0 and the inertial-range estimation $t_0^* = t_I$ mainly differ in the near

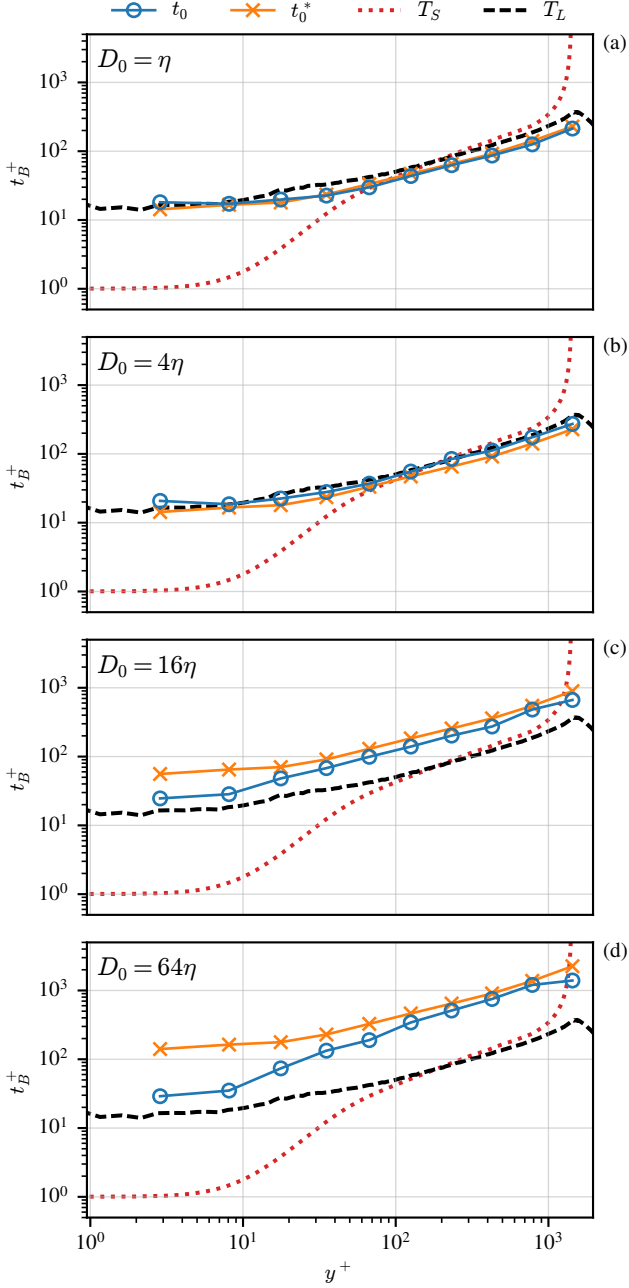


Figure 6: Characteristic relative dispersion time scales in wall units along the channel width, for different initial separations D_0 . From top to bottom, $D_0/\eta = 1, 4, 16$ and 64 . Results were obtained from dataset DS2. Pairs are initially oriented in the spanwise direction ($\mathbf{e}_0 = \mathbf{e}_z$). Circles, $t_0 = \langle \delta \mathbf{v}_0^2 \rangle / |\langle \delta \mathbf{v}_0 \cdot \delta \mathbf{a}_0 \rangle|$; crosses, $t_0^* = \tau_\eta / \beta$ (subfigures a-b) or $t_0^* = \frac{11}{6} C_2 D_0^{2/3} \varepsilon^{-1/3}$ (subfigures c-d). Non-dimensional constants are $C_2 = 2.1$ and $\beta = -0.16$. Also represented are the Lagrangian integral time scale T_L (black dashed line) and the mean shear time scale $T_S = (dU/dy)^{-1}$ (red dotted line).

wall region, and become similar in the bulk of the channel. As suggested by Fig. 5, the difference is explained by a weakly overestimated inertial-range structure function S_2 .

When compared to the Lagrangian integral time scale T_L , t_0 is of the same order of magnitude for small separations, and considerably larger than T_L for larger separations. This implies that scale separation is not achieved in this channel flow and that

an intermediate time range between t_0 and T_L does not exist. As a consequence, Richardson's super-diffusive regime cannot be observed under the present flow conditions.

Finally, it is interesting to compare the ballistic time scale with the characteristic time of the mean shear T_S . As shown in Fig. 6, this time scale is small near the wall, where shear is high, and grows far from the wall as shear decreases. For separations $D_0/\eta = 1$ and 4 , T_S is smaller than t_0 in the near-wall region, up to $y^+ \approx 80$. For larger separations, T_S is smaller than t_0 everywhere in the channel. In these cases, mean shear is expected to influence relative dispersion statistics since the beginning of particle pair separation.

3.4. Normalised mean-square separation

The time scale t_0^* introduced in the previous section is constructed from assumptions on the underlying turbulent flow, namely local homogeneity and isotropy. In contrast, t_0 is obtained according to purely kinematic considerations (without any assumptions on the turbulent flow), and it is chosen here as the characteristic ballistic time scale. Thus, Eq. (2) can be rewritten as

$$\frac{\langle \mathbf{R}^2 \rangle}{\langle \delta \mathbf{v}_0^2 \rangle t_0^2} = \left(\frac{t}{t_0} \right)^2 + s \left(\frac{t}{t_0} \right)^3 + \mathcal{O}(t^4) \quad \text{for } t \ll t_0, \quad (4)$$

where $s \in \{-1, 1\}$ is the sign of $\langle \delta \mathbf{v}_0 \cdot \delta \mathbf{a}_0 \rangle$. In Fig. 7, dispersion curves of Fig. 4 are normalised by the expected ballistic regime according to Eq. (4). Under this scaling, forward dispersion curves associated to different wall distances collapse for times up to $t \approx 2t_0$, emphasising the relevance of the proposed scaling. At longer times, separation is accelerated for pairs that are initially far from the wall. A remarkable t^2 ballistic regime is observed for all wall distances. Starting from $t \approx 0.1t_0$, the mean-square separation deviates from the initial ballistic regime becoming slightly slower for forward dispersion, and faster for backward dispersion, consistently with a negative sign of the t^3 term of Eq. (4). Starting from $y_0^+ = 60$, normalised curves differ only slightly. This is explained by the decay of inhomogeneity and anisotropy far from the wall, resulting in Eulerian velocity and acceleration statistics which evolve similarly with wall distance. In the studied flow, $y^+ = 60$ is located at the beginning of the self-similar logarithmic region (Stelzenmuller et al., 2017).

Figure 8 plots the local scaling exponent of the mean-square separation, i.e., the local slope of the curves shown in Fig. 7. An initial plateau with a value of 2, corresponding to the ballistic regime, is recovered both for forward and backward dispersion. A deviation from this regime is observed as early as $|t|/t_0 \approx 0.01$, and is given by a deceleration of the separation rate in the forward case, and by an acceleration in the backward case (as already seen in Fig. 7). The early deviation from the ballistic regime can be associated to the purely kinematic effect of the t^3 term of Eq. (4) when $s = -1$ (i.e. when $\langle \delta \mathbf{v}_0 \cdot \delta \mathbf{a}_0 \rangle$ is negative). This is confirmed by the comparison between the numerical results and the truncated Taylor expansion of $\langle \mathbf{R}(t)^2 \rangle$ in the figure.

At intermediate times, all cases present an increasing separation rate that ends with a peak. Except for the smallest initial wall distance $y_0^+ = 20$, the peak is found at $2 < |t|/t_0 < 5$. The local scaling exponent reaches larger values in the forward case

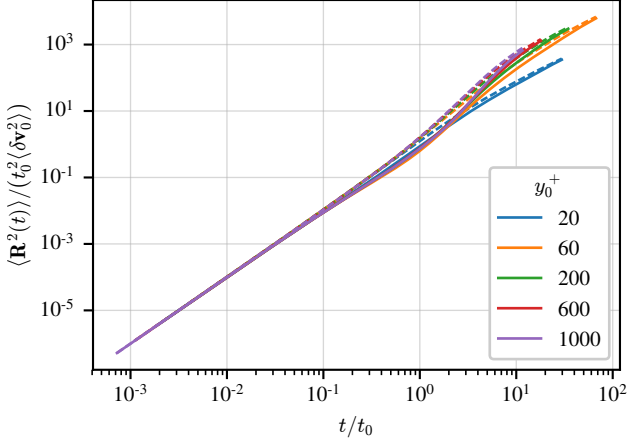


Figure 7: Backward and forward mean-square separation normalised by the structure function $\langle \delta \mathbf{v}_0^2 \rangle$ and the characteristic ballistic time $t_0 = \langle \delta \mathbf{v}_0^2 \rangle / |\langle \delta \mathbf{v}_0 \cdot \delta \mathbf{a}_0 \rangle|$. The initial pair separation is $D_0 < 16\eta$ (dataset DS1). Different colours correspond to different initial wall distances y_0^+ . Solid lines: forward dispersion. Dashed lines: backward dispersion.

than in the backward case. A possible interpretation is that being faster, backward dispersion reaches the normally-diffusive regime earlier than in the case of forward dispersion, thus spending less time in the intermediate super-diffusive regime. At long times, forward and backward separations match, consistently with observations from Fig. 4. In some cases, the local scaling exponents reach values around 3, which is comparable to Richardson's t^3 super-diffusive regime. However, Richardson's regime is not expected to be observed in this flow because of the absence of scale separation and since mean shear is important at early stages of dispersion (as discussed in Section 3.3). Moreover, as seen in Fig. 8, the peaks of the local scaling exponents occur at times larger than the Lagrangian integral time scale T_L . It may be argued that mean shear induces a super-diffusive regime at large times. As stated in the introduction, Pitton et al. (2012) also observed a shear induced super diffusive regime for inertial particle separations of the order of the largest flow scales.

3.5. Temporal asymmetry

The results discussed in Section 3.4 show the temporal asymmetry of relative dispersion in turbulent channel flow. At times following the initial ballistic separation regime, it has been illustrated that backward dispersion is more effective than forward dispersion. As suggested by Jucha et al. (2014), the asymmetry at short times can be explained by subtracting the short-time expansion of the mean-square separation (Eq. 2) for positive and negative times:

$$\langle \mathbf{R}(t)^2 \rangle - \langle \mathbf{R}(-t)^2 \rangle = 2\langle \delta \mathbf{v}_0 \cdot \delta \mathbf{a}_0 \rangle t^3 + \mathcal{O}(t^5) \quad \text{for } t \ll t_0. \quad (5)$$

This difference is plotted in Fig. 9 compensated by $\langle \delta \mathbf{v}_0 \cdot \delta \mathbf{a}_0 \rangle t^3$. As predicted by Eq. (5), a plateau with a value of 2 is initially found for all initial wall distances. A deviation from this plateau is observed starting from $t = 0.05t_0$, which is quantitatively consistent with results in HIT (Jucha et al., 2014). This departure may be due to the neglected t^5 term in Eq. (5), or to particle pairs

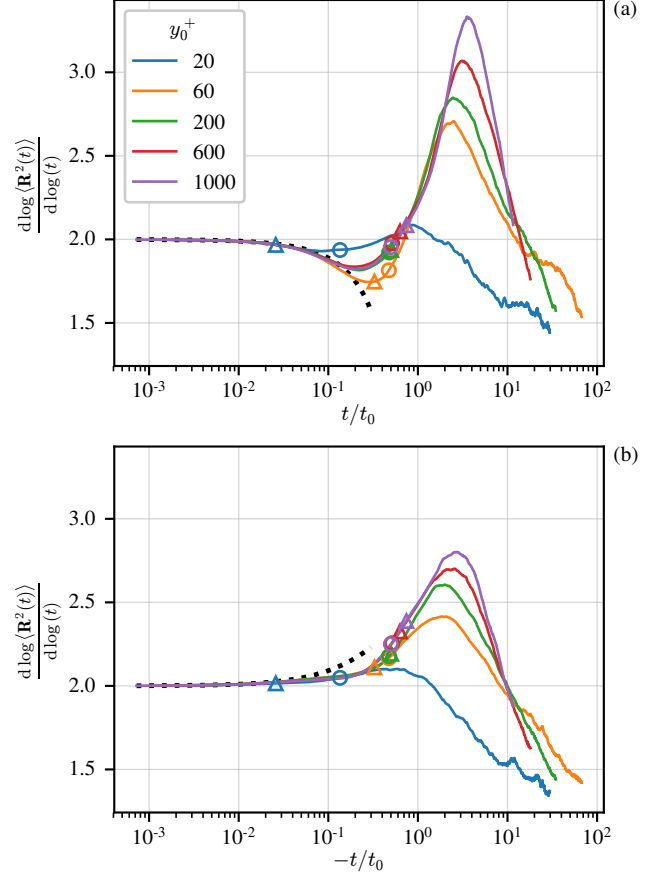


Figure 8: Local scaling exponents of the mean-square separation process. (a) Forward dispersion. (b) Backward dispersion. The dotted line is derived from the truncated Taylor expansion $\langle \mathbf{R}(t)^2 \rangle = \langle \delta \mathbf{v}_0^2 \rangle t^2 + \langle \delta \mathbf{v}_0 \cdot \delta \mathbf{a}_0 \rangle t^3$ with $\langle \delta \mathbf{v}_0 \cdot \delta \mathbf{a}_0 \rangle < 0$. For each initial wall distance y_0^+ , markers indicate the local value of the Lagrangian integral time scale T_L (circles) and of the mean shear time scale T_S (triangles).

sampling the flow at scales larger than D_0 . In the inset of Fig. 9, the difference $\langle \mathbf{R}(-t)^2 \rangle - \langle \mathbf{R}(t)^2 \rangle$ is normalised by the initial mean-square separation $\langle \mathbf{D}_0^2 \rangle$. The positive sign of this difference for all y_0^+ confirms that backward dispersion evolves at faster rate than forward dispersion at all initial positions. Moreover, starting from $y_0^+ = 60$ similarity of the temporal asymmetry with wall distance is observed.

3.6. Influence of the initial separation

The influence of the initial pair configuration, described by the parameters (y_0, \mathbf{D}_0) , on forward relative dispersion is discussed here. As described in Section 3.1, short-time dispersion follows a ballistic regime governed by the second-order Eulerian velocity structure function $S_2(y_0, \mathbf{D}_0)$, described in Section 3.2 for the set of initial pair configurations studied in this work.

In Fig. 10, the mean-square separation is shown for a range of initial wall-normal positions y_0 , separation distances D_0 , and separation orientations \mathbf{e}_0 . As can be predicted from the expression for the short-time regime (Eq. 2) and the structure functions described in Section 3.2, initial orientation plays an important role for particles initialised near the wall (subfigures a-b), while its impact is weaker far from the wall (subfigures

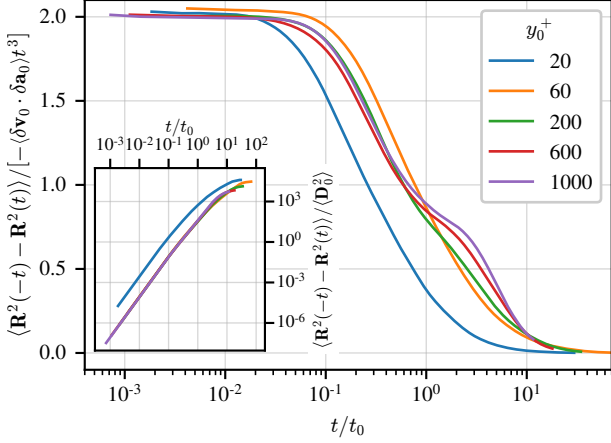


Figure 9: Difference between backward and forward mean-square separation, compensated by $-\langle\delta\mathbf{v}_0 \cdot \delta\mathbf{a}_0\rangle t^3$. Particle pairs are initially separated by $D_0 < 16\eta$ (dataset DS1). Inset: mean-square separation difference compensated by the initial mean-square separation $\langle\mathbf{D}_0^2\rangle$.

c-d). In all cases, the initial ballistic separation is more efficient when the initial separation D_0 is larger. Consistently with the behaviour of the velocity structure functions presented in Fig. 5, anisotropy at short times enhances separation when particles are initially oriented in the wall-normal direction. This has already been observed by Shen and Yeung (1997) in the case of homogeneous turbulent shear flow. The authors found that particles separate faster when they are initially oriented in the cross-stream direction. Furthermore, particles that are oriented in the spanwise direction separate faster than those oriented in the streamwise direction. As discussed in Section 3.2, the presence of streaks and quasi-streamwise vortices near the wall (Robinson, 1991), implies weaker velocity increments between two points aligned in the streamwise direction than in the spanwise direction.

At very long times, the mean-square separation no longer depends on the initial configuration of the pairs. The curves from all the initial configurations collapse due to loss of memory of the initial condition. An intermediate time range connects the initial ballistic regime, strongly dependent on the initial configuration, and the long-time dispersion regime, independent of the initial configuration. The ballistic time scale t_0 (represented by squares over each curve in Fig. 10) is an adequate time scale for representing the transition from the ballistic regime to the intermediate regime. This regime is given by a super-diffusive process which is more efficient than the initial ballistic regime, as already observed in Section 3.4 (for pairs conditioned to an initial separation $|\mathbf{D}_0| < 16\eta$). From Fig. 10, it is found that the slope of the super-diffusive regime is steeper when the initial ballistic regime is slower, that is, when the structure function $S_2(y_0, \mathbf{D}_0)$ is weaker. This is the case for smaller separations $|\mathbf{D}_0|$, and for wall-parallel orientations, when the contribution of mean shear to the structure function S_2 is zero.

4. Mean shear influence

In order to characterise the influence of mean shear on relative dispersion in the channel, we decompose the time evolution

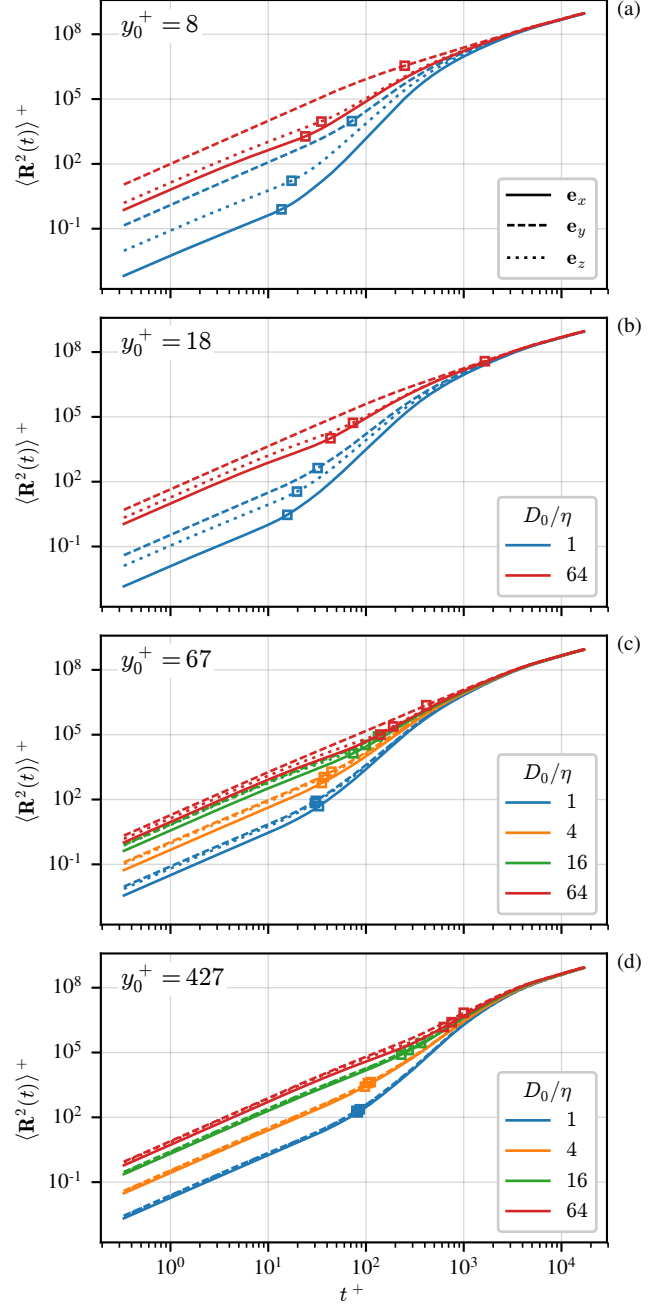


Figure 10: Forward mean-square separation for different initial configurations, in wall units. Pairs are initially located at $y_0^+ = 8, 18, 67$ and 427 (subfigures (a) to (d)). Line styles represent the initial orientation of the pairs: streamwise (solid lines), wall-normal (dashed lines) and spanwise (dotted lines). Line colours represent the initial separation D_0/η . Squares indicate the ballistic time t_0 associated to each initial condition. Results were obtained from dataset DS2.

of the particle pair separation into a separation induced by the mean velocity field, $\bar{\mathbf{R}}(t)$, and a separation due to the fluctuating velocity field, $\mathbf{R}'(t)$. We then study the evolution of the mean-square separation resulting from the fluctuating field $\langle\mathbf{R}'(t)^2\rangle$.

4.1. Decomposition of the mean-square separation

Given an Eulerian mean velocity field $\mathbf{U}(\mathbf{x})$, we define the fluctuating velocity of a fluid particle with trajectory $\mathbf{x}(t)$ as

$\mathbf{v}'(t) = \mathbf{v}(t) - \mathbf{U}(\mathbf{x}(t))$, where $\mathbf{v}(t) = \mathbf{u}(\mathbf{x}(t), t)$ is the total fluid particle velocity. Note that $\mathbf{v}'(t)$ is the fluctuating velocity field at the particle position, $\mathbf{u}'(\mathbf{x}(t), t)$. Correspondingly, a fluctuating acceleration can be defined as

$$\mathbf{a}'(t) = \frac{d\mathbf{v}'(t)}{dt} = \mathbf{a}(t) - \mathbf{v}(t) \cdot \nabla \mathbf{U}(\mathbf{x}(t)), \quad (6)$$

where d/dt is the Lagrangian derivative along the fluid particle path, and $\mathbf{a}(t)$ is the total particle acceleration. In channel flow, the mean velocity field takes the form $\mathbf{U}(\mathbf{x}) = U(y) \mathbf{e}_x$, and therefore Eq. (6) writes

$$\mathbf{a}'(t) = \mathbf{a}(t) - v_y(t) \frac{dU(y(t))}{dy} \mathbf{e}_x, \quad (7)$$

where $y(t)$ and $v_y(t)$ are the wall-normal position and velocity of the particle, respectively.

The increment of instantaneous separation between two particles $\mathbf{R}(t)$ and their relative velocity $\delta\mathbf{v}(t) = \mathbf{v}_2(t) - \mathbf{v}_1(t)$ are then linked by

$$\mathbf{R}(t) = \mathbf{D}(t) - \mathbf{D}_0 = \int_0^t \delta\mathbf{v}(\tau) d\tau \quad (8)$$

$$= \int_0^t \delta\mathbf{U}(\tau) d\tau + \int_0^t \delta\mathbf{v}'(\tau) d\tau \quad (9)$$

$$= \overline{\mathbf{R}}(t) + \mathbf{R}'(t), \quad (10)$$

where $\delta\mathbf{U}(t) = \mathbf{U}(\mathbf{x}_2(t)) - \mathbf{U}(\mathbf{x}_1(t))$ is the mean velocity field difference between the positions $\mathbf{x}_1(t)$ and $\mathbf{x}_2(t)$ of the two particles, such that $\mathbf{D}(t) = \mathbf{x}_2(t) - \mathbf{x}_1(t)$, and $\delta\mathbf{v}'(t) = \mathbf{v}'_2(t) - \mathbf{v}'_1(t)$ is their relative fluctuating velocity.

The time evolution of $\langle \mathbf{R}'^2 \rangle$ is plotted in Fig. 11 for pairs initially separated by $|\mathbf{D}_0| < 16\eta$ and for different initial wall-distances y_0^+ . By comparison to the $\langle \mathbf{R}^2 \rangle$ shown in Fig. 4, the mean-square separation induced by the fluctuating flow is about one order of magnitude weaker than the total mean-square separation at very long times ($t^+ \approx 5000$). When the influence of mean shear is removed, the super-diffusive regime at intermediate times is considerably weaker. Regarding the initial ballistic regime, the difference between $\langle \mathbf{R}^2 \rangle$ and $\langle \mathbf{R}'^2 \rangle$ is more pronounced when pairs are initialised close to the wall. For $y_0^+ = 20$, $\langle \mathbf{R}^2 \rangle$ evolves considerably faster than $\langle \mathbf{R}'^2 \rangle$ during the ballistic regime (that is, $\langle \delta\mathbf{v}_0^2 \rangle > \langle \delta\mathbf{v}'_0^2 \rangle$), as a result of the dominant role of mean shear in the near-wall region. For larger values of y_0^+ , the influence of mean shear on the ballistic regime is much weaker, implying that away from the wall the initial separation regime (and thus the structure function S_2) is governed by turbulent fluctuations.

Similarly to the total relative dispersion described in previous sections, relative dispersion induced by the fluctuating flow is a time-asymmetric process, with backward dispersion being faster than forward dispersion. As before, this asymmetry is first evidenced as a deviation from the initial ballistic separation. The gap between backward and forward dispersion increases at intermediate times, and then decreases at very long times. This confirms that the temporal asymmetry of relative dispersion in turbulent channel flow is a consequence of the irreversibility of turbulent fluctuations, as is in isotropic flows (Jucha et al., 2014).

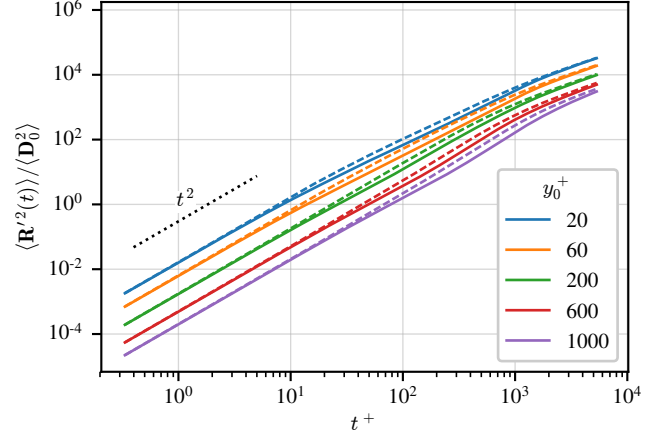


Figure 11: Backward and forward mean-square separation due to the fluctuating flow $\langle \mathbf{R}'^2 \rangle$, normalised by the initial mean-square separation $\langle \mathbf{D}_0^2 \rangle$. Particle pairs are initially separated by $D_0 < 16\eta$ (dataset DS1). Different colours correspond to different initial wall distances y_0^+ . Solid lines: forward dispersion. Dashed lines: backward dispersion.

4.2. Short-time dispersion

Similarly to Eq. (2), the short-time evolution of the mean-square separation due to the fluctuating flow can be written as

$$\langle \mathbf{R}'^2 \rangle(y_0, \mathbf{D}_0, t) = \langle \delta\mathbf{v}'_0{}^2 \rangle t^2 + \langle \delta\mathbf{v}'_0 \cdot \delta\mathbf{a}'_0 \rangle t^3 + O(t^4) \quad \text{for } t \ll t'_0, \quad (11)$$

where $\delta\mathbf{v}'_0 = \delta\mathbf{v}'(0)$ and $\delta\mathbf{a}'_0 = \delta\mathbf{a}'(0)$. Here $\delta\mathbf{a}'(t) = \mathbf{a}'_2(t) - \mathbf{a}'_1(t)$ is the relative fluctuating acceleration of the particles. Thus, the separation $\mathbf{R}'(t)$ is also expected to follow an initial ballistic growth, although the characteristic duration of this ballistic regime is not necessarily the same as for the total change of separation $\mathbf{R}(t)$. From the above expression and according to the discussion in Section 3.3, the ballistic time scale associated to \mathbf{R}' is defined as $t'_0 = \langle \delta\mathbf{v}'_0{}^2 \rangle / |\langle \delta\mathbf{v}'_0 \cdot \delta\mathbf{a}'_0 \rangle|$.

The local scaling exponent of $\langle \mathbf{R}'(t)^2 \rangle$ is shown in Fig. 12 with time normalised by t'_0 . As with $\langle \mathbf{R}(t)^2 \rangle$ (shown in Fig. 4), for all wall distances the initial ballistic regime is followed by a decelerated separation in the forward case and by an accelerated separation in the backward case, which are both explained by a negative value of $\langle \delta\mathbf{v}'_0 \cdot \delta\mathbf{a}'_0 \rangle$ in Eq. (11). The observed behaviour closely follows the truncated Taylor expansion of $\langle \mathbf{R}'(t)^2 \rangle$ at short times. As it was observed from Fig. 11, the super-diffusive regime at intermediate times is remarkably weaker for $\langle \mathbf{R}'(t)^2 \rangle$ than for the total separation $\langle \mathbf{R}(t)^2 \rangle$ (see Fig. 8), with maximum values that barely exceed the initial ballistic scaling $\langle \mathbf{R}'^2 \rangle \sim t^2$. This confirms that the intermediate super-diffusive regime that was found in previous sections, described by an instantaneous scaling reaching $\langle \mathbf{R}^2 \rangle \sim t^3$, is due to mean shear and not to Richardson's law. At very long times, the average separation rate decelerates continuously. It may be predicted that the diffusion due to the fluctuating flow should tend to a normally-diffusive process, as in HIT (Taylor, 1922), which would correspond to a scaling $\langle \mathbf{R}'^2 \rangle \sim t$. However, the available data is insufficient to verify this statement.

Analogously to Eq. (5), the temporal asymmetry of $\langle \mathbf{R}'(t)^2 \rangle$

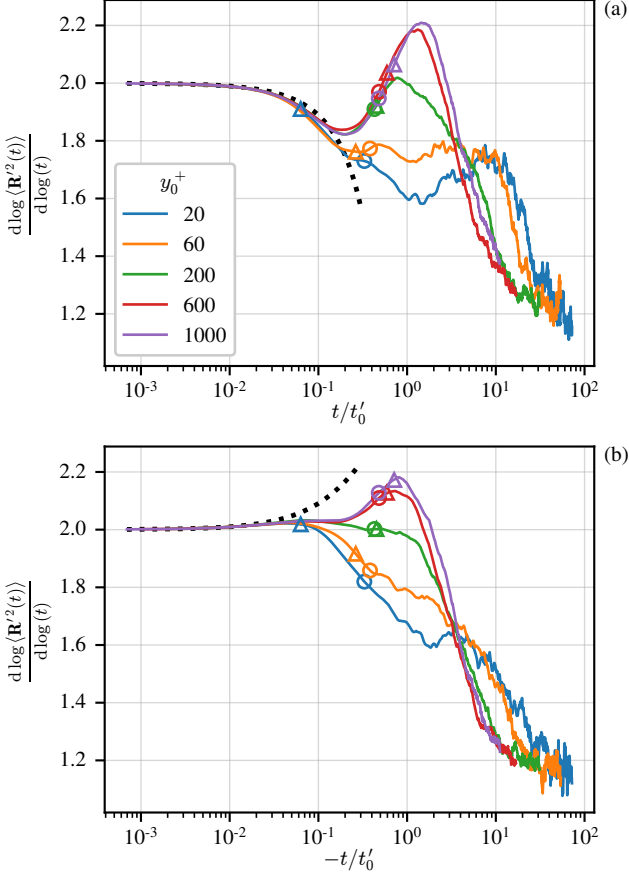


Figure 12: Local scaling exponents of the mean-square separation by the fluctuating flow $\langle \mathbf{R}'(t)^2 \rangle$. (a) Forward dispersion. (b) Backward dispersion. The dotted line is derived from the truncated Taylor expansion $\langle \mathbf{R}'(t)^2 \rangle = \langle \delta \mathbf{v}'_0 \cdot \delta \mathbf{a}'_0 \rangle t^2 + \langle \delta \mathbf{v}'_0 \cdot \delta \mathbf{a}'_0 \rangle t^3$ with $\langle \delta \mathbf{v}'_0 \cdot \delta \mathbf{a}'_0 \rangle < 0$. For each initial wall distance y_0^+ , markers indicate the local value of the Lagrangian integral time scale T_L (circles) and of the mean shear time scale T_S (triangles).

can be described at short times by

$$\langle \mathbf{R}'(t)^2 \rangle - \langle \mathbf{R}'(-t)^2 \rangle = 2 \langle \delta \mathbf{v}'_0 \cdot \delta \mathbf{a}'_0 \rangle t^3 + O(t^5) \quad \text{for } t \ll t_0'. \quad (12)$$

The validity of this analytical prediction is verified from simulation data in Fig. 13, where the difference $\langle \mathbf{R}'(t)^2 \rangle - \langle \mathbf{R}'(-t)^2 \rangle$ is plotted compensated by $\langle \delta \mathbf{v}'_0 \cdot \delta \mathbf{a}'_0 \rangle t^3$. The expected plateau at 2 is recovered for times $t \lesssim 0.1 t_0'$, similarly to the case of the total mean-square separation $\langle \mathbf{R}^2 \rangle$ (Fig. 9), and consistently with equivalent results in HIT (Jucha et al., 2014; Bragg et al., 2016). Namely, in the case of HIT, Jucha et al. (2014) compared the compensated difference as given in Fig. 13 obtained from DNS with experimental data at four different Reynolds numbers ranging from $Re_\lambda = 200$ to 690. All their data showed a clear plateau up to $t \approx t_0/10$, in complete agreement with equation (12). Here, the plateau ranges up to $t \approx t_0'/20$ for different wall distances and even close to the wall, where anisotropy increases. Interestingly, for $y_0^+ = 20$, the plateau is present and the curve matches the behaviour at higher wall distances, which was not the case for $\langle \mathbf{R}^2 \rangle$ shown in Fig. 9. More generally, the spread of the curves associated to different y_0^+ is reduced with respect to that obtained from the total mean-square separation $\langle \mathbf{R}^2 \rangle$ (Fig. 9), emphasising

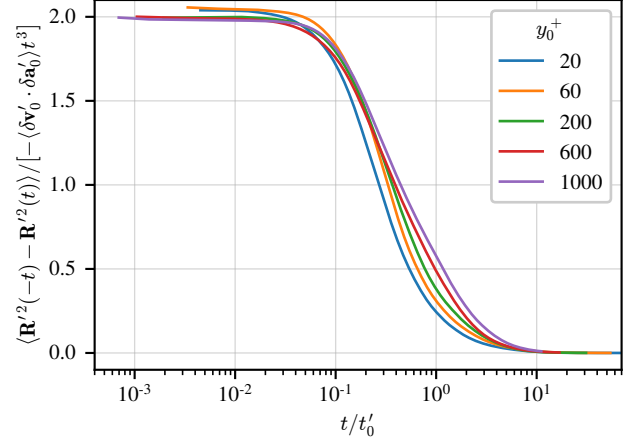


Figure 13: Difference between backward and forward mean-square separation due to the fluctuating flow, compensated by $-\langle \delta \mathbf{v}'_0 \cdot \delta \mathbf{a}'_0 \rangle t^3$. Results were obtained from dataset DS1.

the impact of mean shear on $\langle \mathbf{R}^2 \rangle$, at relatively short times close to the wall and at larger times away from the wall. As mentioned in Section 2, the initial wall distance of particles in the $y_0^+ = 20$ set is within $0 \leq y^+ \leq 40$. Therefore, the current study does not allow for a finer description of the temporal asymmetry of pair dispersion close to the wall.

Figure 14 plots the difference $\langle \mathbf{R}'(-t)^2 \rangle - \langle \mathbf{R}'(t)^2 \rangle$ compensated by the initial mean-square separation $\langle \mathbf{D}_0^2 \rangle$. As in Fig. 9, all the curves display a positive sign associated to backward dispersion being faster than forward dispersion. Similarity of the results is found for all initial wall distances including $y_0^+ = 20$. Moreover, a common long-time limit is observed. This limit is characterised by a plateau starting at $t \approx 10 t_0'$, suggesting that the temporal asymmetry of dispersion is enhanced during the short-time separation regime, and then becomes negligible at long times. The dotted lines in Fig. 14 represent the forward-backward dispersion difference in each Cartesian direction (i.e. the contribution of each separation component to Eq. (12)), for particles initially located at $y_0^+ \approx 600$. In this case, backward dispersion is faster than forward dispersion in every direction. At long times, the time asymmetry of the dispersion is most pronounced in the streamwise direction.

In the case of a mean shear turbulent flow, Celani et al. (2005) estimated the time required for two particles to reach separations at which the mean shear and the turbulent fluctuations contributions become comparable. According to the authors, this time scale t_c is inversely proportional to the mean shear, and therefore directly proportional to $T_S = (dU(y)/dy)^{-1}$. In turbulent channel flow, as y^+ increases, mean shear decreases and the time scale at which mean shear and turbulent fluctuations present comparable contributions increases. This is confirmed by the results in Fig. 10 since the squares on the curves representing the ballistic time scale t_0 move to the right as the wall distance increases.

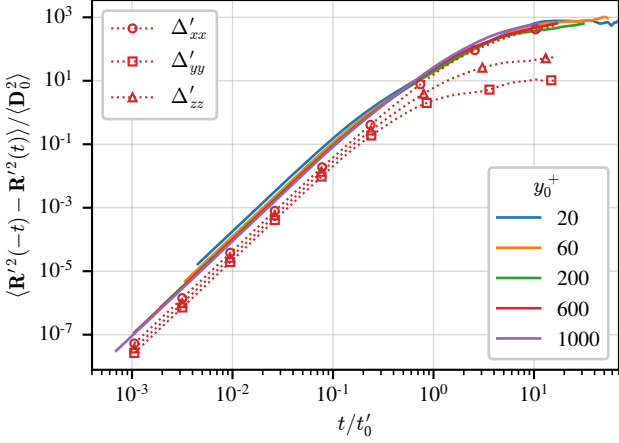


Figure 14: Difference between forward and backward mean-square separation due to the fluctuating flow, compensated by $\langle D_0^2 \rangle$. Results were obtained from dataset DS1. Dotted lines represent the directional decomposition associated to dispersion tensor components Δ'_{xx} (circles), Δ'_{yy} (squares) and Δ'_{zz} (triangles), for pairs in the $y_0^+ = 600$ set.

5. Relative dispersion tensor

Until now, we have considered statistics related to the change of separation magnitude between a pair of particles, $|\mathbf{R}(t)| = |\mathbf{D}(t) - \mathbf{D}_0|$. However, the separation between two particles in inhomogeneous and anisotropic flows presents an anisotropic evolution in time. Namely, the presence of mean shear enhances particle separation in the streamwise direction, while it does not have a direct effect in the other directions.

The anisotropy of relative dispersion can be investigated by means of the relative dispersion tensor (Batchelor, 1952; Monin and Yaglom, 1975),

$$\Delta_{ij}(t) = \langle R_i(t)R_j(t) \rangle, \quad (13)$$

where $R_i(t) = D_i(t) - D_i(0)$ is the i -th component of $\mathbf{R}(t)$. The trace of Δ_{ij} is equal to the mean-square separation, $\Delta_{ii}(t) = \langle \mathbf{R}(t)^2 \rangle$. By construction, Δ_{ij} is a symmetric tensor. In channel flow, due to the statistical symmetry $z \leftrightarrow -z$, its non-diagonal components Δ_{xz} and Δ_{yz} are zero. As a consequence, the relative dispersion tensor contains a single independent non-diagonal component, $\Delta_{xy} = \Delta_{yx}$. Each component of the relative dispersion tensor depends on the initial wall distance y_0 and on the initial particle separation vector \mathbf{D}_0 .

The short-time evolution of $\langle \mathbf{R}(t)^2 \rangle$ as predicted by Eq. (2) can be generalised to

$$\Delta_{ij}(y_0, \mathbf{D}_0, t) = \langle \delta v_{0i} \delta v_{0j} \rangle t^2 + (\langle \delta v_{0i} \delta a_{0j} \rangle + \langle \delta v_{0j} \delta a_{0i} \rangle) \frac{t^3}{2} + O(t^4) \quad \text{for } t \ll t_0. \quad (14)$$

Therefore, each component of Δ_{ij} independently follows an initial ballistic regime according to the velocity structure function tensor $\langle \delta v_{0i} \delta v_{0j} \rangle = S_{ij}(\mathbf{x}_0, \mathbf{D}_0) = \overline{\delta u_i(\mathbf{x}_0, \mathbf{D}_0) \delta u_j(\mathbf{x}_0, \mathbf{D}_0)}$. At the next order, the t^3 term is governed by the symmetric part of the crossed velocity-acceleration structure function tensor $\langle \delta v_{0i} \delta a_{0j} \rangle = \overline{\delta u_i(\mathbf{x}_0, \mathbf{D}_0) \delta a_j(\mathbf{x}_0, \mathbf{D}_0)}$.

Due to wall confinement, particle separation in the wall-normal direction cannot exceed $|D_y| = 2h$. It is possible to estimate, at sufficiently long times, the influence of confinement on the wall-normal mean-square separation $\langle D_y^2 \rangle$. Under the assumption of loss of memory of the initial particle position, the wall-normal position of a single particle can be expected to follow a uniform distribution at long times, described by the probability density function (PDF) $P_y(y) = 1/(2h)$ for $0 \leq y \leq 2h$. Moreover, the trajectories of two particles in a pair are expected to decorrelate over a sufficiently long time, implying that the joint PDF describing the wall-normal positions of the two particles, $P_{yy}(y_1, y_2)$, writes as $P_y(y_1)P_y(y_2)$. Under these assumptions, the wall-normal mean-square separation is given by

$$\langle D_y^2 \rangle \equiv \int_0^{2h} \int_0^{2h} (y_2 - y_1)^2 P_{yy}(y_1, y_2) dy_1 dy_2 = \frac{2}{3} h^2. \quad (15)$$

This equation is also an estimation for the wall-normal component of the dispersion tensor, i.e. $\Delta_{yy} \approx 2h^2/3$ at long times, under the additional assumption that the initial wall-normal separation is small compared to the channel dimensions, i.e. $|D_{0y}| \ll h$.

5.1. Short-time dispersion

In Fig. 15, the temporal evolution of the relative dispersion tensor is shown for particle pairs initially located at different wall-distances y_0 . In all cases, pairs are initially separated in the spanwise direction by $D_0 = 16\eta$. Because of the spanwise alignment of the pairs, mean shear does not play a role during the initial ballistic separation. As predicted by Eq. (14), the ballistic regime is observed for each component of Δ_{ij} . Pair dispersion is anisotropic since the start of the separation. During the ballistic regime, for the shown initial configurations, particles near the wall separate faster in the streamwise direction, while separation is slowest in the wall-normal direction. For the nearest wall distances ($y_0^+ = 8$ and 18), this means that the streamwise separation dominates the total separation from the start, which is confirmed by the superposition between the curves for Δ_{xx} and $\langle \mathbf{R}^2 \rangle$ at all times. By DNS in a homogeneous turbulent shear flow, Shen and Yeung (1997) also found that particle-pair dispersion is most effective in the streamwise direction, as already stated in the introduction. In turbulent channel flow, the rapid streamwise separation at short times for particles initially separated in the spanwise direction may be explained by the presence of near-wall streaks. These are elongated regions in the streamwise direction, carrying low-speed and high-speed fluid alternating in the spanwise direction (Robinson, 1991). Two particles initially belonging to two neighbouring streaks (a high-speed streak next to a low-speed streak), experience a rapid streamwise separation due to the velocity difference between the streaks.

As expected, the short-time behaviour approaches isotropy as particles are released further away from the wall. In all cases, for each of the three diagonal components, the ballistic separation is immediately followed by a deceleration of the separation rate. Following Eq. (14), and consistently with the observations from previous sections, this deceleration is associated with a

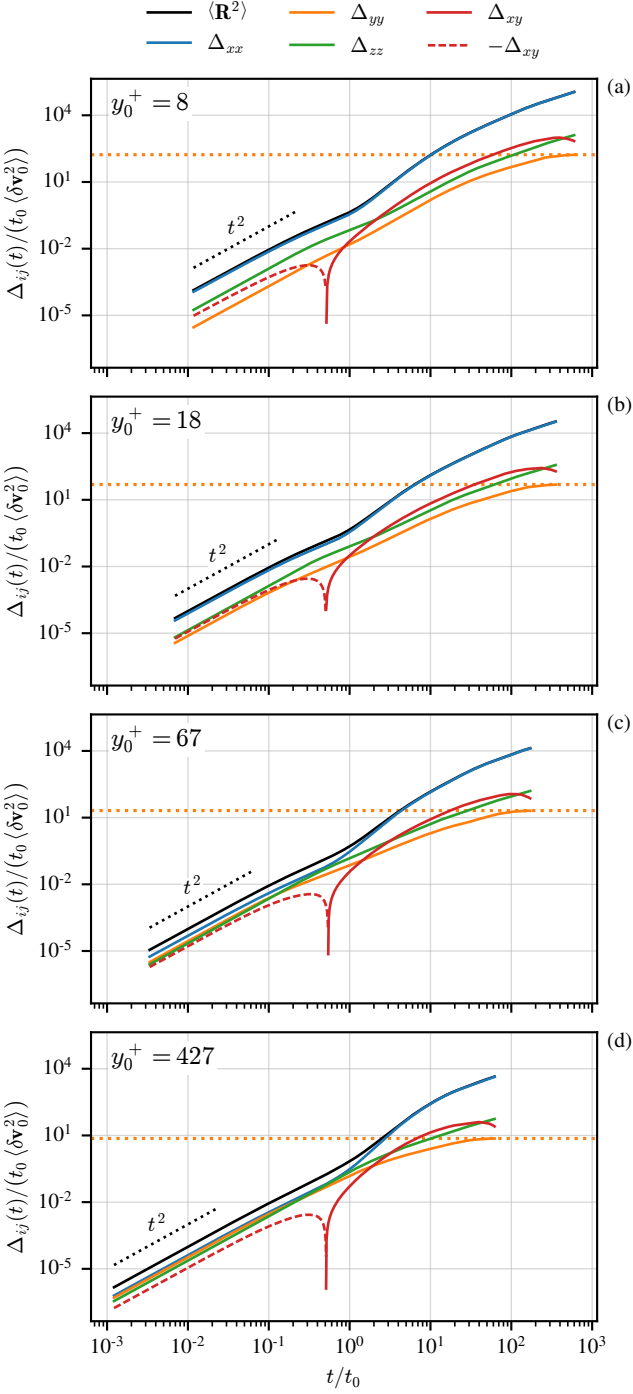


Figure 15: Components of the relative dispersion tensor, normalised by the structure function $\langle \delta v_0^2 \rangle$ and the characteristic ballistic time t_0 . Particle pairs are initially located at $y_0^+ = 8, 18, 67$ and 427 (subfigures (a) to (d)). Pairs are initially oriented in the spanwise direction (z), with a separation $D_0 = 167\eta$. The total mean-square separation $\Delta_{ii} = \langle \mathbf{R}^2 \rangle$ is also represented. The dotted horizontal line marks the level $\Delta_{ij} = 2h^2/3$, where h is the channel half-width. Results were obtained from dataset DS2.

negative value of the component-wise crossed structure functions $\langle \delta v_{0i} \delta a_{0i} \rangle$ (where repeated indices do not imply summation).

5.2. Intermediate and long-time dispersion

At intermediate times starting from $t \approx t_0$, Δ_{xx} displays an accelerated separation rate, while Δ_{yy} and Δ_{zz} evolve at slower rates compared to the initial ballistic regime. The rapid separation in the streamwise direction can be attributed to the effect of mean shear. The duration of this rapid separation regime, which lasts until $t \approx 10t_0$, is consistent with the duration of the super-diffusive regime observed for $\langle \mathbf{R}^2 \rangle$ in Fig. 8a and discussed in Section 4.

The estimation $\Delta_{yy} \approx 2h^2/3$ accurately predicts the wall-normal pair separation at long times. This prediction is valid starting from $t^+ \approx 10^4$ for all initial wall distances y_0^+ (not shown here). As noted in Section 3.6, Fig. 10, for $t^+ \approx 10^4$ the mean-square separation no longer depends on the initial pair configuration.

5.3. Time evolution of cross-term Δ_{xy}

Finally, the time evolution of the cross-term Δ_{xy} may yield additional insight on the mechanisms of pair separation in wall-bounded turbulence. Initially, Δ_{xy} evolves ballistically with an increasingly negative value at all wall distances, which following Eq. (14) corresponds to a negative value of the structure function $\langle \delta v_{0x} \delta v_{0y} \rangle$. This is consistent with the model of Yang et al. (2017), predicting a structure function S_{xy}^+ between -1 and -2 when y_0 and $y_0 + D_{0y}$ are within the logarithmic region. The ballistic regime ends with a deviation of Δ_{xy} towards positive values, resulting from a positive value of the t^3 term in Eq. (14). This leads to a change of sign of Δ_{xy} , that becomes positive at $t \approx t_0/2$ for all initial wall distances.

At intermediate times, Δ_{xy} displays a rapid growth, coinciding with the super-diffusive growth of Δ_{xx} . As for Δ_{xx} , this is due to the influence of mean shear. To illustrate this, we consider a pair of particles A and B initially located in the lower half of the channel ($0 < y_0 < h$). At some point, even if the particles are initially close, their wall-normal separation $|D_y| = |y_B - y_A|$ will grow due to turbulent diffusion until $|D_y|$ becomes large enough for mean shear effects to be important. Without loss of generality, we assume that particle B is further away from the wall than particle A, i.e. $D_y > 0$. Therefore, as long as the particles have not yet crossed the channel centre, particle B is located in a region of faster average flow than A, and thus their streamwise separation $D_x = x_B - x_A$ grows rapidly due to the mean shear. The result is a product $D_x D_y$ which rapidly grows over time as long as D_y remains positive. This is no longer valid once a particle crosses the channel centre, leading to the decelerated growth of Δ_{xy} at later times.

6. Ballistic dispersion model

Relative dispersion statistics in turbulent channel flow may be reproduced using a simple model based on the ballistic cascade phenomenology proposed by Bourgoin (2015) to describe relative dispersion in isotropic turbulent flows. Bourgoin (2015)

explained the transition from the short-term ballistic separation to Richardson's super-diffusive regime ($\langle \mathbf{R}^2 \rangle \sim t^3$) at long times as a temporal progression of discrete, short-lived ballistic separations. This approach is similar to previous models (Sokolov et al., 2000; Faber and Vassilicos, 2009; Thalabard et al., 2014), all of which considered the relevance of successive ballistic separations on pair dispersion. In the following, we briefly present Bourgoïn's ballistic cascade model in the case of 3D isotropic turbulent flows. Then, we propose and test a modified model that takes into account mean shear in the case of turbulent channel flows.

6.1. Ballistic cascade model in isotropic turbulence

Bourgoïn (2015) formulated the ballistic cascade in isotropic turbulence as a simple iterative model. Starting from an initial separation D_0 within the inertial subrange, the mean-square separation $\langle \mathbf{D}^2 \rangle$ is incremented at each iteration by a ballistic assumption according to:

$$D_{k+1}^2 = D_k^2 + S_2(D_k) t_k'^2(D_k) \quad \text{for } k = 0, 1, 2, \dots, \quad (16)$$

where D_k^2 is the mean-square separation at iteration k . Here, $S_2(D_k) = \frac{11}{3} C_2 (\varepsilon D_k)^{2/3}$ is the isotropic second-order Eulerian velocity structure function for D_k in the inertial subrange, as introduced in Section 3.1. The duration of the k -th iteration is given by $t_k' = \alpha t_k$, where $t_k = S_2(D_k)/(2\varepsilon)$ is a characteristic time of the ballistic regime (equal to t_I as defined in Section 3.3), and α is a non-dimensional constant referred to as the persistence parameter. The total time elapsed by the start of iteration k is $T_k = \sum_{j=0}^{k-1} t_j'(D_j)$.

Besides Kolmogorov's constant C_2 , which has the well-accepted value $C_2 \approx 2.1$ (Sreenivasan, 1995), α is the only free parameter of the model. By analytically relating C_2 and α to Richardson's constant, Bourgoïn (2015) found $\alpha = 0.12$ as the value that best matches the well-accepted Richardson constant in 3D turbulence, $g \approx 0.55$ (Ott and Mann, 2000; Bitane et al., 2012). With this value of the persistence parameter, the ballistic cascade model has been shown to reproduce with great accuracy the DNS results from Bitane et al. (2012) in HIT at a Taylor-scale Reynolds number $Re_\lambda = 730$, with initial particle separations D_0 ranging between 2η and 48η .

The model described by Eq. (16) is symmetric in time. Bourgoïn (2015) also proposed a time-asymmetric version of the model by taking into account the t^3 term in the Taylor expansion (2), associated with the velocity-acceleration structure function S_{au} . This refined model captures a ratio between backward and forward Richardson constant $g_{\text{bw}}/g_{\text{fw}} = 1.9$, consistent with available experimental and DNS results.

6.2. Ballistic cascade model in inhomogeneous turbulence

As shown in previous sections, the mean-square separation of particle pairs in channel flow is accurately described at short times by an average ballistic separation. Therefore, a model based on a succession of ballistic separations may seem suitable for predicting pair dispersion statistics in the studied flow. In the following, such a model is proposed based on Bourgoïn's approach, which is adapted to account for the effect of an

inhomogeneous mean velocity field $\mathbf{U}(\mathbf{x})$. The model is also adjusted to take into account the transition from inertial to integral-scale separations at sufficiently long times. In addition to the mean velocity field, the present model requires as input the mean turbulent dissipation rate $\varepsilon(\mathbf{x})$. The model is started with an initial pair separation vector \mathbf{D}_0 and with the initial position of the pair centroid, $\tilde{\mathbf{x}} = (\mathbf{x}_0^A + \mathbf{x}_0^B)/2$, where \mathbf{x}_0^A and \mathbf{x}_0^B are the initial positions of the two particles. In channel flow, due to homogeneity in the streamwise and spanwise directions, the model requirements reduce to the mean streamwise velocity profile along the channel $U(y)$ and the turbulent dissipation profile $\varepsilon(y)$, as well as the initial particle configuration given by \mathbf{D}_0 and the wall-normal centroid position $\tilde{y}_0 = (y_0^A + y_0^B)/2$.

We model the time evolution of the mean-square separation vector $\langle \mathbf{D}^2 \rangle$ and the position of the pair centroid $\tilde{\mathbf{x}}$ iteratively. As a first approximation, the centroid position is kept fixed over time, i.e. $\tilde{\mathbf{x}}_k = \tilde{\mathbf{x}}_0$ at every iteration k . This will be improved in future versions of the model, by taking into account the drift of the particle pair centroid based on single-particle dispersion statistics. At iteration k , the mean-square separation in each direction $i \in \{x, y, z\}$ is incremented according to

$$D_{k+1,i}^2 = D_{k,i}^2 + S_{2i}(\tilde{\mathbf{x}}_k, \mathbf{D}_k) t_k'^2(\tilde{\mathbf{x}}_k, \mathbf{D}_k) \quad \text{for } k = 0, 1, 2, \dots, \quad (17)$$

where $D_{k,i}^2$ is the mean-square separation in the i -th direction at iteration k . The total mean-square separation is then $D_k^2 = D_{k,x}^2 + D_{k,y}^2 + D_{k,z}^2$. The structure function S_{2i} is associated to the velocity component u_i , and can be written as the superposition of a mean and a fluctuating component:

$$S_{2i}(\tilde{\mathbf{x}}_k, \mathbf{D}_k) = \bar{S}_{2i}(\tilde{\mathbf{x}}_k, \mathbf{D}_k) + S'_{2i}(\tilde{\mathbf{x}}_k, \mathbf{D}_k). \quad (18)$$

The mean component is readily obtained from the mean velocity field:

$$\bar{S}_{2i}(\tilde{\mathbf{x}}_k, \mathbf{D}_k) = \left[U_i \left(\tilde{\mathbf{x}}_k + \frac{\mathbf{D}_k}{2} \right) - U_i \left(\tilde{\mathbf{x}}_k - \frac{\mathbf{D}_k}{2} \right) \right]^2. \quad (19)$$

The fluctuating component S'_{2i} is estimated so as to account for the transition from inertial to integral-scale separations. For separations within the inertial range, S'_{2i} is estimated from HIT as (Pope, 2000):

$$S_{2i}^I(\tilde{\mathbf{x}}_k, \mathbf{D}_k) = C_2 \left(\varepsilon(\tilde{\mathbf{x}}_k) |\mathbf{D}_k| \right)^{2/3} \left(\frac{4}{3} - \frac{1}{3} \frac{D_{k,i}^2}{|\mathbf{D}_k|^2} \right). \quad (20)$$

In HIT, the structure function $S_2(D_0)$ tends to $2\sigma_u^2$ for integral-scale separations, over which the velocity field becomes fully decorrelated in space. Here σ_u^2 is the variance of the velocity fluctuations. Consistently, the present model estimates S'_{2i} for separations within the integral scales as

$$S_{2i}^L(\tilde{\mathbf{x}}_k, \mathbf{D}_k) = 2\sigma_i^2(\tilde{\mathbf{x}}_k), \quad (21)$$

where $\sigma_i^2 = u_i'^2$ is the variance of the velocity component u_i . It is reasonable to model S'_{2i} as an increasing function of the spatial increment $|\mathbf{D}_{k,i}|$. Therefore, a straightforward way of estimating

the fluctuating component of the velocity structure function is to take

$$S'_{2i}(\tilde{\mathbf{x}}_k, \mathbf{D}_k) = \min \{ S_{2i}^I(\tilde{\mathbf{x}}_k, \mathbf{D}_k), S_{2i}^L(\tilde{\mathbf{x}}_k, \mathbf{D}_k) \}. \quad (22)$$

According to this expression, the transition from inertial to integral separations is implicit, since it happens once the inertial-range prediction S_{2i}^I becomes larger than S_{2i}^L . A weakness of this model is that the scale transition happens abruptly, whereas the structure function should be a smooth function of the separation. According to the present model, the three components of the separation \mathbf{D} may transition to the integral scales at different times. This is not a problem since, in inhomogeneous flows, the integral scales generally depend on the considered orientation.

As in the original model by Bourgoïn (2015), the iteration time is taken as $t'_k = \alpha t_k$, with the ballistic time scale estimated as $t_k(\tilde{\mathbf{x}}_k, \mathbf{D}_k) = S'_2(\tilde{\mathbf{x}}_k, \mathbf{D}_k)/(2\varepsilon(\tilde{\mathbf{x}}_k))$. Here, the structure function S'_2 is given by $S'_2(\tilde{\mathbf{x}}_k, \mathbf{D}_k) = \sum_{i=1}^3 S'_{2i}(\tilde{\mathbf{x}}_k, \mathbf{D}_k)$. The value of the persistence parameter $\alpha = 0.12$ is kept unchanged. Finally, the time elapsed by the start of iteration k is given by $T_k = \sum_{j=0}^{k-1} t'_j(\tilde{\mathbf{x}}_j, \mathbf{D}_j)$. When the mean velocity field is constant, mean shear is neglected and the present model falls back to the isotropic model described above when separations are in the inertial subrange.

The present model does not account for the presence of solid boundaries. In the case of channel flow, this implies that wall confinement is not accounted for. Hence, the present model allows particles to travel beyond the channel walls. As implied by Eq. (19), the model effectively estimates the absolute wall-normal position of the two particles as $y_k = \tilde{y}_k \pm D_{k,y}/2$, where \tilde{y}_k is the wall-normal position of the pair centroid. When one of the particles crosses the channel walls, its mean velocity is taken as $\mathbf{U} = 0$. In future work wall confinement will be accounted for thoroughly. We present here preliminary findings of a very simple extension of the original ballistic model in HIT.

The proposed simple model is tested in the channel flow configuration, using as input a mean velocity profile $U(y)$, a turbulent dissipation profile $\varepsilon(y)$, and velocity variance profiles $\overline{u_i^2}(y)$ obtained from our DNS at $Re_\tau = 1440$. We test two initial configurations, corresponding to initial particle locations $y_0^+ = 67$ and 427 . In both cases, the initial particle separation is $\mathbf{D}_0 = 16\eta\mathbf{e}_z$. The DNS results corresponding to these cases were already analysed in the previous sections (see for instance Fig. 15). Since the present model includes elements from isotropic turbulence, its results are expected to be more accurate for particles initialised far from the walls, where anisotropy is weaker. The chosen initial separation $D_0 = 16\eta$ is rather favourable for testing the model since, as shown in Fig. 5, the structure function S_2 closely matches the expected inertial-range behaviour from HIT for this initial separation. For smaller separations such as $D_0/\eta = 1$ and 4 , the model should be extended by including the dissipation-range structure functions as estimated in Section 3.2.

A comparison between the model and the DNS results is shown in Fig. 16 for the two chosen initial configurations. Also shown is a variant of the model with a zero mean velocity profile ($U(y) = 0$). As mentioned above, this is equivalent to neglecting the effect of mean shear on dispersion. Furthermore, since

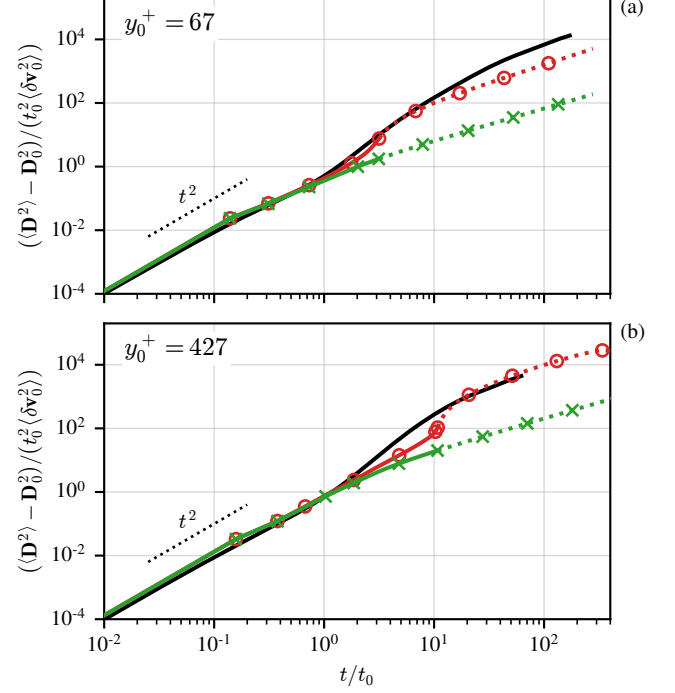


Figure 16: Inhomogeneous ballistic cascade model compared to channel flow DNS results. Particle pairs are initially located at (a) $y_0^+ = 67$ and (b) $y_0^+ = 427$. In both cases, the initial pair separation is $D_0 = 16\eta$ in the spanwise direction. Black line, DNS results; circles, ballistic model with velocity profile $U(y)$; crosses, ballistic model with constant velocity profile. The dotted part of the model curves correspond to the results once one of the particles has traversed the channel walls.

the mean turbulent dissipation ε does not vary in time in the inhomogeneous model (because the particle pair centroid $\tilde{\mathbf{x}}$ does not move), the model variant is actually equal to the homogeneous model by Bourgoïn (2015) as long as the separations $D_{k,i}$ stay within the inertial subrange.

As shown in the Fig. 16, during the first few ballistic iterations both versions give quite satisfactory predictions compared to the DNS results. Model predictions up to $t \approx 3t_0$ closely follow the DNS results for the initial wall distance $y_0^+ = 67$. Up to $t \approx t_0$, the two versions of the model show a similar behaviour, implying the absence of mean shear influence. Still, the models closely predict a deceleration of pair separation after the initial ballistic regime. Moreover, the full model predicts the start of the super-diffusive regime that follows, although it does not precisely capture the time at which this regime starts being observed. The model with zero velocity profile does not show evidence of Richardson's t^3 regime due to a lack of scale separation, since particle pairs do not spend enough time in the inertial subrange.

Ongoing work is dedicated to a more refined model that partially accounts for wall confinement through the particle pair centroid trajectory, which is pushed away from solid boundaries. At long times, when the memory of the initial particle position is lost, the particle pair centroid is expected to be located, in average, at the channel centre. The present model will also be extended to account for the inter-dependency between separation directions. This will be quantified by the non-diagonal components of the relative dispersion tensor described in Section 5. The

model described by Eq. (17) will then be rewritten according to a tensor formulation. In channel flow, this requires the estimation of the crossed velocity structure function $S_{xy}(y, \mathbf{D}) = \delta u_x(\mathbf{x}, \mathbf{D}) \delta u_y(\mathbf{x}, \mathbf{D})$.

7. Conclusions

This work deals with forward and backward dispersion statistics of fluid particle pairs in a turbulent channel flow obtained by direct numerical simulations. Relative dispersion statistics are conditioned to a wide range of initial configurations. Each configuration is given by an initial separation, orientation, and wall distance of an ensemble of particle pairs.

Irrespective of the initial pair configuration, the mean-square particle separation at short times is accurately described by the Eulerian structure of the flow at the initial configuration, namely by the second-order velocity structure function $S_2(y_0, \mathbf{D}_0)$ and the crossed velocity-acceleration structure function $S_{au}(y_0, \mathbf{D}_0)$. The characteristic time scale derived from these two statistics has been shown to represent the duration of the short-time regime. The initial ballistic regime is typically driven by turbulent fluctuations. However, when the initial wall-normal separation is larger than the local characteristic shear length scale, the influence of mean shear on the separation rate is evidenced.

The short-time evolution is followed by a shear-driven super-diffusive regime. Its scaling is highly dependent on the initial particle configuration. Namely, the separation rate in this regime is most important in cases where mean shear does not play a role at short times (for small initial separations, or for initial orientations parallel to the wall). Conversely, when shear affects the ballistic regime, the intermediate regime presents lower separation rates.

Consistently with similar studies in isotropic turbulence, particle pairs separate faster in average when followed backwards than forwards in time. At short times, this time asymmetry is associated with a negative sign of S_{au} . The asymmetric behaviour persists when only the separation by the fluctuating flow is considered, confirming that the observed time asymmetry is a consequence of turbulence irreversibility.

The anisotropy of relative dispersion has been characterised by studying the relative dispersion tensor Δ_{ij} . The dominant role of mean shear is described by an increased growing rate of the streamwise mean-square separation Δ_{xx} and of the cross-term Δ_{xy} during the intermediate regime that follows ballistic growth. Conversely, the wall-normal and spanwise diagonal terms Δ_{yy} and Δ_{zz} display a decelerated growth following the ballistic regime.

Finally, a simple relative dispersion model has been introduced based on the ballistic cascade phenomenology proposed by Bourgoin (2015) for isotropic flows. The present model accounts for the effect of mean shear on pair separation, while keeping strong isotropic assumptions of the original model. When particle pairs are initialised away from the wall, with initial separations within the inertial range, the model closely predicts the mean-square separation obtained from channel flow DNS over short times. Later, the model predicts the accelerated separation of

particles due to mean shear, although the quantitative comparison with the DNS data remains unsatisfactory. In future developments of the inhomogeneous model, wall confinement effects on particle displacement will be accounted for.

One of the most prominent features of wall-bounded turbulent flows are near-wall streamwise vortices, responsible for ejections and sweeps. The role of these particular structures on the short-time dispersion of particle pairs will be examined in future studies. Forthcoming studies will also deal with Lagrangian dispersion of fluid particle tetrads and analysis of four-point velocity difference statistics.

Acknowledgements

This work has been supported by Agence Nationale de la Recherche (Grant No. ANR-13-BS09-0009). Simulations have been performed on the P2CHPD cluster of the Fédération Lyonnaise de Sciences Numériques and the national computing centre CINES (grant no. DARI A0022A07707). J.I.P. is grateful for CONICYT Becas Chile Grant No. 72160511 for supporting his work.

References

- Angevine, W. M., Brioude, J., McKeen, S., Holloway, J. S., Lerner, B. M., Goldstein, A. H., Guha, A., Andrews, A., Nowak, J. B., Evan, S., Fischer, M. L., Gilman, J. B., Bon, D., Jun. 2013. Pollutant transport among California regions. *J. Geophys. Res. Atmospheres* 118 (12), 6750–6763.
- Batchelor, G. K., Apr. 1950. The application of the similarity theory of turbulence to atmospheric diffusion. *Q.J.R. Meteorol. Soc.* 76 (328), 133–146.
- Batchelor, G. K., Apr. 1952. Diffusion in a field of homogeneous turbulence: II. The relative motion of particles. *Math. Proc. Cambridge Philos. Soc.* 48 (2), 345–362.
- Berg, J., Lüthi, B., Mann, J., Ott, S., Jul. 2006. Backwards and forwards relative dispersion in turbulent flow: An experimental investigation. *Phys. Rev. E* 74 (1), 016304.
- Biferale, L., Boffetta, G., Celani, A., Devenish, B. J., Lanotte, A., Toschi, F., Nov. 2005. Lagrangian statistics of particle pairs in homogeneous isotropic turbulence. *Phys. Fluids* 1994–Present 17 (11), 115101.
- Bitane, R., Homann, H., Bec, J., Oct. 2012. Time scales of turbulent relative dispersion. *Phys. Rev. E* 86 (4), 045302.
- Bourgoin, M., Jun. 2015. Turbulent pair dispersion as a ballistic cascade phenomenon. *J. Fluid Mech.* 772, 678–704.
- Bragg, A. D., Ireland, P. J., Collins, L. R., Jan. 2016. Forward and backward in time dispersion of fluid and inertial particles in isotropic turbulence. *Phys. Fluids* 28 (1), 013305.
- Buaria, D., Sawford, B. L., Yeung, P. K., Oct. 2015. Characteristics of backward and forward two-particle relative dispersion in turbulence at different Reynolds numbers. *Phys. Fluids* 1994–Present 27 (10), 105101.
- Buffat, M., Le Penven, L., Cadiou, A., Mar. 2011. An efficient spectral method based on an orthogonal decomposition of the velocity for transition analysis in wall bounded flow. *Comput. Fluids* 42 (1), 62–72.
- Celani, A., Cencini, M., Vergassola, M., Villiermaux, E., Vincenzi, D., Jan. 2005. Shear effects on passive scalar spectra. *J. Fluid Mech.* 523, 99–108.
- Davidson, P. A., Krogstad, P.-A., Aug. 2014. A universal scaling for low-order structure functions in the log-law region of smooth- and rough-wall boundary layers. *J. Fluid Mech.* 752, 140–156.
- de Silva, C. M., Marusic, I., Woodcock, J. D., Meneveau, C., Apr. 2015. Scaling of second- and higher-order structure functions in turbulent boundary layers. *J. Fluid Mech.* 769, 654–686.
- Faber, T., Vassilicos, J. C., Jan. 2009. Turbulent pair separation due to multiscale stagnation point structure and its time asymmetry in two-dimensional turbulence. *Phys. Fluids* 21 (1), 015106.

- Fornari, W., Picano, F., Brandt, L., Jan. 2018. The effect of polydispersity in a turbulent channel flow laden with finite-size particles. *Eur. J. Mech. B.* 67, 54–64.
- Frisch, U., Nov. 1995. *Turbulence: The Legacy of A. N. Kolmogorov*. Cambridge University Press.
- Fung, J. C. H., Lau, A. K. H., Lam, J. S. L., Yuan, Z., May 2005. Observational and modeling analysis of a severe air pollution episode in western Hong Kong. *J. Geophys. Res.* 110 (D9), D09105.
- Hill, R. J., Jan. 2006. Opportunities for use of exact statistical equations. *J. Turbul.* 7, N43.
- Hoffmann, L., Rößler, T., Griessbach, S., Heng, Y., Stein, O., May 2016. Lagrangian transport simulations of volcanic sulfur dioxide emissions: Impact of meteorological data products. *J. Geophys. Res. Atmospheres* 121 (9), 4651–4673.
- Jucha, J., Xu, H., Pumir, A., Bodenschatz, E., Jul. 2014. Time-reversal-symmetry Breaking in Turbulence. *Phys. Rev. Lett.* 113 (5).
- Kolmogorov, A. N., 1941. The local structure of turbulence in incompressible viscous fluid for very large Reynolds numbers. *Dokl Akad Nauk SSSR* 30, 301–305.
- Koszalka, I., LaCasce, J. H., Orvik, K. A., Jul. 2009. Relative dispersion in the Nordic Seas. *Journal of Marine Research* 67 (4), 411–433.
- LaCasce, J. H., 2010. Relative displacement probability distribution functions from balloons and drifters. *J. Mar. Res.* 68 (3-1), 433–457.
- Lashgari, I., Picano, F., Breugem, W. P., Brandt, L., Jan. 2016. Channel flow of rigid sphere suspensions: Particle dynamics in the inertial regime. *Int. J. Multiph. Flow* 78, 12–24.
- Lozano-Durán, A., Jiménez, J., Jan. 2014. Effect of the computational domain on direct simulations of turbulent channels up to $Re\tau = 4200$. *Phys. Fluids* 1994-Present 26 (1), 011702.
- Lumpkin, R., Elipot, S., Dec. 2010. Surface drifter pair spreading in the North Atlantic. *J. Geophys. Res.* 115 (C12).
- Mann, J., Ott, S., Andersen, J. S., Sep. 1999. Experimental study of relative, turbulent diffusion. Technical report Risø-R-1036(EN), Risø National Laboratory, Roskilde, Denmark.
- Monin, A. S., Yaglom, A. M., 1975. *Statistical Fluid Mechanics: Mechanics of Turbulence*, 2nd Edition. Vol. 2. MIT Press, Cambridge, oCLC: 245996380.
- Obukhov, A. M., 1941. On the distribution of energy in the spectrum of turbulent flow. *Izv Akad Nauk SSSR* 5, 453–66.
- Ott, S., Mann, J., Nov. 2000. An experimental investigation of the relative diffusion of particle pairs in three-dimensional turbulent flow. *J. Fluid Mech.* 422, 207–223.
- Pitton, E., Marchioli, C., Lavezzo, V., Soldati, A., Toschi, F., 2012. Anisotropy in pair dispersion of inertial particles in turbulent channel flow. *Phys. Fluids* 24 (7), 073305.
- Pope, S. B., Aug. 2000. *Turbulent Flows*. Cambridge University Press.
- Rast, M. P., Pinton, J.-F., Nov. 2011. Pair Dispersion in Turbulence: The Subdominant Role of Scaling. *Phys. Rev. Lett.* 107 (21), 214501.
- Richardson, L. F., 1926. Atmospheric Diffusion Shown on a Distance-Neighbour Graph. *Proc. R. Soc. Lond. Ser. A* 110 (756), 709–737.
- Robinson, S. K., 1991. Coherent motions in the turbulent boundary layer. *Annu. Rev. Fluid Mech.* 23 (1), 601–639.
- Salazar, J. P. L. C., Collins, L. R., 2009. Two-Particle Dispersion in Isotropic Turbulent Flows. *Annu. Rev. Fluid Mech.* 41 (1), 405–432.
- Sardina, G., Schlatter, P., Brandt, L., Picano, F., Casciola, C. M., May 2012. Wall accumulation and spatial localization in particle-laden wall flows. *J. Fluid Mech.* 699, 50–78.
- Sawford, B., 2001. Turbulent relative dispersion. *Annu. Rev. Fluid Mech.* 33 (1), 289–317.
- Sawford, B. L., Yeung, P. K., Borgas, M. S., 2005. Comparison of backwards and forwards relative dispersion in turbulence. *Phys. Fluids* 17 (9), 095109.
- Shen, P., Yeung, P. K., Nov. 1997. Fluid particle dispersion in homogeneous turbulent shear flow. *Phys. Fluids* 1994-Present 9 (11), 3472–3484.
- Smits, A. J., McKeon, B. J., Marusic, I., Jan. 2011. High-Reynolds Number Wall Turbulence. *Annu. Rev. Fluid Mech.* 43 (1), 353–375.
- Sokolov, I. M., Klafter, J., Blumen, A., Mar. 2000. Ballistic versus diffusive pair dispersion in the Richardson regime. *Phys. Rev. E* 61 (3), 2717–2722.
- Sreenivasan, K. R., Nov. 1995. On the universality of the Kolmogorov constant. *Phys. Fluids* 7 (11), 2778–2784.
- Stanislas, M., Oct. 2017. Near wall turbulence: An experimental view. *Phys. Rev. Fluids* 2 (10), 100506.
- Stelzenmüller, N., Polanco, J. I., Vignal, L., Vinkovic, I., Mordant, N., May 2017. Lagrangian acceleration statistics in a turbulent channel flow. *Phys. Rev. Fluids* 2 (5), 054602.
- Taylor, G. I., 1922. Diffusion by continuous movements. *Proc Lond. Math. Soc.* s2-20 (1), 196–212.
- Thalabard, S., Krstulovic, G., Bec, J., Sep. 2014. Turbulent pair dispersion as a continuous-time random walk. *J. Fluid Mech.* 755.
- Toschi, F., Bodenschatz, E., Jan. 2009. Lagrangian Properties of Particles in Turbulence. *Annu. Rev. Fluid Mech.* 41 (1), 375–404.
- Townsend, A. A., 1976. *The Structure of Turbulent Shear Flow*. Cambridge University Press, Cambridge [England]; New York, oCLC: 1937010.
- Yang, X. I. A., Baidya, R., Johnson, P., Marusic, I., Meneveau, C., Jun. 2017. Structure function tensor scaling in the logarithmic region derived from the attached eddy model of wall-bounded turbulent flows. *Phys. Rev. Fluids* 2 (6), 064602.
- Yeo, K., Kim, B.-G., Lee, C., Sep. 2010. On the near-wall characteristics of acceleration in turbulence. *J. Fluid Mech.* 659, 405–419.